Supplementary Information

AmAT19, an acetyltransferase from *Astragalus membranaceus*, catalyzes specific 6*α*-OH acetylation for tetracyclic triterpenes and steroids

Linlin Wang [a], Kuan Chen [a], Zilong Wang [a], Yang Yi [a], Meng Zhang [a], Aobulikasimu Hasan [a], Yi Kuang [a], Sharpkate Shaker [a], Rong Yu [a], Haotian Wang [a], Haiyang Liu [b], Min Ye*[a], Xue Qiao*[a]

[a] State Key Laboratory of Natural and Biomimetic Drugs, School of Pharmaceutical Sciences, Peking University, 38 Xueyuan Road, Beijing 100191, China

[b] State Key Laboratory of Phytochemistry and Plant Resources in West China and Yunnan Key Laboratory of Natural Medicinal Chemistry, Kunming Institute of Botany, Chinese Academy of Sciences, Kunming 650201, China

* Corresponding authors. Email address: yemin@bjmu.edu.cn (M. Ye), or qiaoxue@bjmu.edu.cn (X. Qiao).

1. Experimental procedures

1.1 General remarks

The compounds Cycloastragenol (**1**), (20*R*,24*S*)-6*α*,16*β*,25-trihydroxy-20,24-epoxycycloartan-3-onecyclopycnanthogenin (**9**), (20*R*,24*S*)-2*α*,3*β*,6*α*,16*β*,25-pentahydroxy-20,24-epoxy-cycloartane (**10**), (20*R*,24*S*)-3*β*,6*α*,16*β*,25,28-pentahydroxy-20,24-epoxycycloartane (**11**), (3*β*,6*α*,11*β*,16*β*,24*S*)-20,24-Epoxy-11-(hydroxymethyl)-19-norlanost-9-ene-3,6,16,25-tetrol (**12**), and (*E*)-3*β*,6*α*-dihydroxy-lanost-9(11),17(20),22(23)-triene-24-one (**13**) were biotransformation productions of cycloastragenol by *Syncephalastrum racemosum* and *Alternaria alternata* as previously reported [1]. Hyodeoxycholic acid (**3**) was purchased from Energy Chemical (Shanghai China). Taurohyodeoxycholic acid (**15**) was purchased from Honghu Lianhe (Beijing, China). Glycine hyodeoxycholic acid (**16**) and *α*-murocholic acid (**18**) were purchased from Bide Pharmatech (Shanghai China). 5α-Androstane-3β,6α,17β-triol (**20**) was purchased from Leyan (Shanghai China). Protopanaxatriol (**2**), Ginsenoside Rg1 (**15**), Ginsenoside Rh1 (**14**), ginsenoside F1 (**6**), astragaloside IV (**16**), protopanaxadiol (**17**), madecassic acid (**8**), glycyrrhetinic acid (**21**), and oleanolic acid (**22**) were purchased from Desite (Chengdu, China). Murideoxycholic acid (**15**) was purchased from Zhongkaiboya (Beijing, China). 6*α*-*O*-*β*-D-Glucopyranosyl-(20*S*,24*R*)-epoxydammarane-3*β*,12*β*,25-triol (**12**) was prepared in our lab as previously reported [2].

Methanol and acetonitrile (UPLC grade) were purchased from Fisher Scientific (USA). Acetyl-CoA, malonyl-CoA, benzoyl-CoA, *p*-coumaroyl-CoA, and caffeoyl-CoA were purchased from Sigma-Aldrich (St. Louis, MO, USA). The analysis of the reaction mixture was analyzed by Vanquish™ UHPLC coupled with Q-Exactive HRMS

(Thermo Fisher, CA, USA), and HPLC (SSI-III) coupled with ELSD 6000 (Alletch Chrom, USA). NMR spectra were recorded on a Bruker AVANCE III-600 instrument at 600 MHz for ^{1}H and 150 MHz for ^{13}C in pyridine-d_5, or a Bruker AVANCE III-400 instrument at 400 MHz for ^{1}H and 100 MHz for ^{13}C in pyridine-d_5. Chemical shifts (δ) are given in parts per million (ppm). and coupling constants (J) are given in hertz (Hz).

1.2 Plant materials

We purchased the *A. membranaceus* seeds from Anguo FengHua Seed Station (Hebei, China), and confirmed its species by DNA barcoding using *psbA-trnH* fragments [3].

1.3 Molecular phylogenetic analysis

The evolutionary history was inferred by using the Maximum Likelihood method based on the JTT matrix-based model [9]. The tree with the highest log likelihood (-7275.97) is shown. The percentage of trees in which the associated taxa clustered together is shown next to the branches. Initial tree(s) for the heuristic search were obtained automatically by applying Neighbor-Join and BioNJ algorithms to a matrix of pairwise distances estimated using a JTT model, and then selecting the topology with superior log likelihood value. The tree is drawn to scale, with branch lengths measured in the number of substitutions per site. The analysis involved 25 amino acid sequences. All positions containing gaps and missing data were eliminated. There were a total of 181 positions in the final dataset. Evolutionary analyses were conducted in MEGA7 [10].

1.4 Molecular cloning, heterologous expression and protein purification

We extracted the total RNA from the seedlings by using the TranZol™ kit (TransGen Biotech, China) and reverse-transcribed to cDNA using the FastQuant RT Kit (Tiangen

Biotech, China). The open reading frame was amplified using specific primers. The amplification product was cloned into a pET-28a (+) vector (Invitrogen, USA) by Quick-change (Tiangen Biotech, China). After sequencing, the recombined plasmid pET-28a-AmAT19 was transformed into *E. coli* BL21 (DE3) (TransGen Biotech, China) for expression. The *E. coli* cells were grown in Luria-Bertani (LB) medium containing 50 μg/mL kanamycin at 37 °C until the OD_{600} reached 0.6. Then, isopropyl *β*-D-thiogalactoside (IPTG, 0.1 mM) was added, and the cells were grown for another 20 h at 16 °C. After expression, the cells were centrifuged at 8000 rpm for 10 min at 4 °C and resuspended in 15 mL of lysis buffer (pH 8.0, 50 mM NaH_2PO_4, 30 mM NaCl, 10 mM imidazole). The collected cells were disrupted through ultrasonic on ice for 10 min and centrifuged for 45 min at 12000 rpm at 4 °C. Subsequently, the protein was purified by Ni-column (Proteinlso Ni-NTA Resin, TransGen Biotech, Beijing, China) and concentrated using Amicon Ultra-15 Ultracel-30K centrifuge filters (Merck Millipore). The concentrated proteins were used as purified recombinant enzymes. The recombinant AmAT19 determined by SDS-PAGE is shown in Figure S2.

1.5 Optimization of reaction system and kinetic studies

To optimize the reaction time of AmAT19, we analyzed the reaction mixture at 0-30 min. To optimize the reaction buffer and pH, we used various reaction buffers with different pH from 4.0-6.0 (citric acid-sodium citrate buffer), 6.0-8.0 (Na_2HPO_4-NaH_2PO_4 buffer), 7.0-9.0 (Tris-HCl buffer), and added 10μg of enzyme into the reaction system. To optimize the reaction temperature, we used different temperatures from 0-75°C, and added 2μg of enzyme into the reaction system. To optimize the influence of metal ions, we added 5 mM of Ba^{2+}, Ca^{2+}, Cu^{2+}, Fe^{2+}, Mn^{2+}, Ni^{2+}, Zn^{2+} and EDTA respectively, and added 10μg of enzyme into the reaction system. All the

reactions used acetyl-coenzyme A as acyl donors and cycloastragenol (**1**) as the acyl acceptor. The reactions were stopped through adding 200 μL of methanol into the system. Then, the mixture was concentrated to dryness and reconstituted with 200 μL of methanol and centrifuged at 15000 rpm for 20 min for further analysis. The results were shown in Figure S3.

For kinetic studies of Am AT19, the assay was performed in a final volume of 50 μL Na_2HPO_4- NaH_2PO_4 (pH 6.0), consisting of 0.016875 μg AmAT19, 2 mM of saturating acetyl coenzyme A, and different concentrations of compound **1** (5, 10, 20, 40, 60, 80, 100 μM). The mixture was incubated at 30 °C for 10 min and quenched with 100 μL of ice cold MeOH. Michaelis-Menten plot was fitted (Figure S4).

1.6 UHPLC/MS methods for analytical reactions

The samples were separated on a Waters T3 column (2.1×150 mm, 1.8 μm) for UHPLC/MS analysis. The mobile phase consisted of 0.1% formic acid (*v*/*v*, A) and methanol (B). The column temperature was 50 °C. Gradient program: 0-1 min, 8% B; 1-19 min, 8%-47% B; 10-16 min, 47%-65% B; 16-19 min, 65%-100% B; 19-22 min, 100% B; 22-25 min, 8% B. The flow rate was 0.3 mL/min. MS analysis was performed on a Q-Exactive hybrid quadrupole-orbitrap mass spectrometer (Thermo Scientific, San Jose, USA) equipped with a heated electrospray ionization source (HESI) in both positive ion mode and negative ion mode. MS parameters: spray voltage: ±3.5 kV; capillary temperature: 350 °C; sheath gas: 45 arb; aux gas: 10 arb; probe heater temperature: 400 °C; S-lens RF level: 60 V; resolution: 70000 for full MS and 17500 for MS/MS; scan range: m/z 100-1200; stepped NCE: 35 eV. Data were processed using Xcalibur™ 4.1 software (Thermo Fisher Scientific).

1.7 HPLC/ELSD methods for analytical reactions

The samples were analyzed on an Agilent Zorbax SB C_{18} column (4.6×250 mm, 5 μm) protected with a Zorbax Extend-C_{18} guard column (4.6 ×12.5 mm, 5 μm). The mobile phase consisted of 0.01% trifluoroacetic acid (*v*/*v*, A) and acetonitrile (B). Gradient program: 0-10 min, 30%-70% B; 10-20 min, 70%-100% B; 20-25 min, 100% B; 25-30 min, 30% B. The flow rate was 1 mL/min. ELSD analysis was performed on a ELSD 6000 (Alletch Chrom, USA). Parameters: temperature 106 °C; gas flow 2.9 L/min. Data were processed using CSChrom Plus software (Laballiance, USA).

1.8 Substrate and donor promiscuity

To detect the substrate heterogeneity of AmAT19, we tested compounds **1-22** as acyl acceptors when acetyl coenzyme A was used as the as acetyl donor. The acyl donor promiscuity was tested using five different donors (acetyl-, malonyl-, benzoyl-, caffeoyl-, and courmanyl-coenzyme A) when cyclogalegenol (**1**) and hyodeoxycholic acid (**3**) were used as acceptors. Reactions were carried out in an 100-μL mixture containing 50 mM NaH_2PO_4-Na_2HPO_4 (pH 6.0), 0.5 mM acetyl donor, 0.1 mM acetyl acceptor, 10 μg purified protein and 10 mM rac-dithiothreitol (DTT). The reaction mixtures were incubated at 30°C for 10 minutes before adding 200 μL of methanol to stop the reaction. The samples were pre-treated and analyzed using UHPLC/MS or HPLC/ELSD as described in Supporting information 1.6-1.7.

1.9 Preparation of acetylated products

To prepare compound **3a**, 500 mg (1.27 mM) of compound **3** was dissolved in 2 mL of pyridine, then acetic anhydride (1.27 mM) was added into the mixture. The mixture

was stirred under nitrogen protection overnight at room temperature before adding 5 mL of ethyl acetate to stop the reaction. The resulted mixture was washed by 1N HCl (5 mL), saturated sodium bicarbonate (5 mL), and saturated sodium chloride solution (5 mL) successively. Then the ethyl acetate layer was concentrated to dryness, redissolved by methanol, and pre-purified by normal-phase TLC (mobile phase: dichloromethane: methanol=20:1). The silica gel containing the acetylated product was extracted by ultrasonication for 20 min × 3 times, and the supernatant was collected and concentrated to dryness. The compound was then purified by HPLC/ELSD by isocratic elution using 50% water (containing 0.01% trifluoroacetic acid) and 50% acetonitrile. The preparation of standard **2a**/**4a** was the same as **3a**, except for the isocratic elution for HPLC/ELSD was 38% B for **4a** and 60% B for **2a**. The products were identified by HRMS and NMR.

1.10 Screening of 3CL^{pro} protein inhibitory activity

The inhibitors of 3CL^{pro} protein were screened using a model of fluorescence resonance energy transfer (FRET) [4]. The system contained 12.5 μg/mL 3CL^{pro} protein, 3 mM Dabcyl-KTSAVLQSGFRKME-Edans (peptide substrate, Edans as the fluorescent donor), 8 μM test compound, and 20 mM Tris-HCl buffer (pH 7.0). The mixture was incubated at 25 °C for 10 min. The fluorescence intensity was detected at 340 nm excitation light and 490 nm emitted light by a fluorescence microplate reader (FlexStation 3 (Molecular Devices, USA)). The 3CL^{pro} protein inhibitory activity was calculated using the follow equation:

$$A = \frac{\Delta OD_{test}}{\Delta OD_{control}\left(2.204092 \times C \times V_S\right)}$$

A: 3CL^{pro} protein inhibitory activity of the test molecules; ΔOD: absorbance change

rate; C: Final concentration of the protein; V_S: final volume of the solution; Test: test compound; Control: control group adding equal volume of solvent.

1.11 HRMS, ^{1}H and ^{13}C NMR data of compounds 2a, 3a and 4a

Protopanaxatriol-6-*O*-acetate (2a): white, amorphous powder. ^{1}H-NMR (600 MHz, pyridine-*d5*) δ: 1.41 (1H, m, H-5), 5.69 (1H, m, H-6), 3.47 (1H, m, H-3), 1.77 (1H, d, Ha-7), 1.84 (1H, m, Hb-7), 2.13 (3H, s, H-Ac-CH_3). ^{13}C-NMR (150 MHz, pyridine-*d5*) δ: 39.3 (C-1), 28.2 (C-2), 77.8 (C-3), 40.0 (C-4), 59.5 (C-5), 71.3 (C-6), 43.4 (C-7), 41.5 (C-8), 50.3 (C-9), 40.0 (C-10), 32.2 (C-11), 71.1 (C-12), 48.6 (C-13), 51.9 (C-14), 31.6 (C-15), 27.1 (C-16), 55.1 (C-17), 17.7 (C-19), 73.3 (C-20), 27.4 (C-21), 36.1 (C-22), 23.3 (C-23), 126.6 (C-24), 131.2 (C-25), 18.0 (C-26), 26.2 (C-27), 31.6 (C-28), 17.0 (C-29),170.0 (C-1'), 22.3 (C-2').

Hyodeoxycholic acid-6-*O*-acetate (3a): white, amorphous powder; HRESIMS *m/z* 433.2956 $[M-H]^-$ (calcd. for $C_{26}H_{41}O_5$, 433.2959, Δ=0.7 ppm). ^{1}H-NMR (600 MHz, pyridine-d_5) δ: 1.88 (1H, m, H-5), 5.32 (1H, m, H-6), 3.85 (1H, m, H-3), 1.70 (1H, m, H-7), 1.35 (1H, m, H-7), 2.06 (3H, s, H-Ac-CH_3).^{13}C-NMR (150 MHz, pyridine-d_5) δ: 36.0 (C-1), 30.9 (C-2), 70.6 (C-3), 28.3 (C-4), 45.9 (C-5), 71.6 (C-6), 36.3 (C-7), 34.8 (C-8), 40.1 (C-9), 36.3 (C-10), 20.9 (C-11), 40.0 (C-12), 42.9 (C-13), 56.1 (C-14), 24.2 (C-15), 31.2 (C-16), 56.0 (C-17), 12.2 (C-18), 23.4 (C-19), 35.6 (C-20), 18.5 (C-21), 31.8 (C-22), 32.1 (C-23), 175.5 (C-24), 170.2 (C-1'), 21.2 (C-2'). [5,6].

5*α*-androstane-3*β*,6*α*,17*β*-triol-6-*O*-acetate (4a): white, amorphous powder; HRESIMS *m/z* 351.2514 $[M+H]^+$ (calcd. for $C_{21}H_{34}O_4$, 351.2530, Δ=4.6 ppm). ^{1}H-

NMR (400 MHz, pyridine-*d5*) δ: 1.40 (1H, m, H-5), 5.02 (1H, m, H-6), 3.85 (1H, m, H-3), 2.14 (1H, m, H-7), 1.06 (1H, m, H-7), 2.06 (3H, s, H-Ac-CH_3). ^{13}C-NMR (100 MHz, pyridine-*d5*) δ: 37.4 (C-1), 31.5 (C-2), 70.8 (C-3), 21.5 (C-4), 49.8 (C-5), 73.0 (C-6), 33.7 (C-7), 35.0 (C-8), 54.5 (C-9), 38.3 (C-10), 21.5 (C-11), 37.7 (C-12), 44.0 (C-13), 51.5 (C-14), 24.0 (C-15), 31.3 (C-16), 81.6 (C-17), 12.3 (C-18), 13.9 (C-19), 170.9(C-1'), 21.5 (C-2') [7].

Supplementary Table

Table S1 The primers for *AmAT19* gene.

Primers	Sequences (5'to 3')
AmAT19-F	GGGTCGCGGATCCGAATTCGAGCTCATGGATATCGAAATAGTCTCCACTC
AmAT19-R	CTCGAGTGCGGCCGCAAGCTTGTCGACCATACATGCATAAGGATTTGGATC

Supplementary Figures

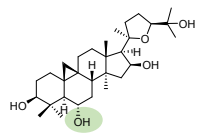

cycloastragenol

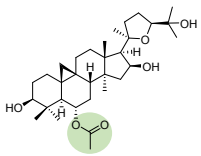

cycloastragenol-6-*O*-acetate

enhanced the Nrf2 activation

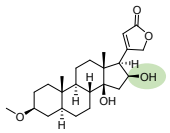

3-*O*-methyl 5*α*-oleandrigenin

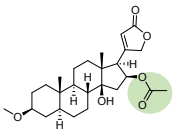

3-*O*-methyl 5*α*-oleandrigenin-16-*O*-acetate

improved the cytotoxicity for oxysterols and the Na^+/K^+-ATP-ase inhibitory activity

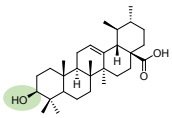

ursolic acid

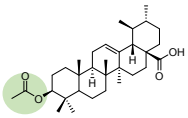

ursolic acid-3-*O*-acetate

anti-plasmodial activity against *Plasmodium falciparum*

Figure S1 Acylation modification of tetracyclic triterpenes and steroids.

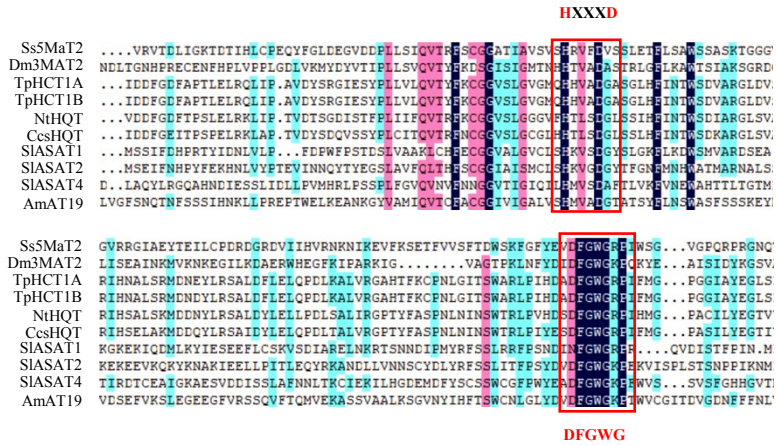

Figure S2 Amino acid sequence alignment for AmAT19 and other plant ATs.

The characteristic conserved motifs were framed in red. Dm3MAT2 (GeneBank accession number AAQ63616); TpHCT1A (GeneBank accession number ACI16630); TpHCT1B (GeneBank accession number ACI28534); NtHQT (GeneBank accession number CAE46932); CcsHQT (GeneBank accession number ABK79689); SlASAT1 (GeneBank accession number ALU64003); SlASAT2 (GeneBank accession number ALU64014); SlASAT4 (GeneBank accession number AFM77971.1); AmAT19 (GeneBank accession number MW803561) [8].

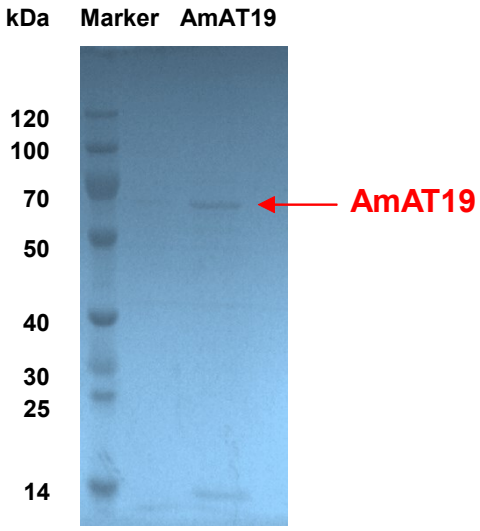

Figure S3 SDS-PAGE of AmAT19 modified with 6×His tag and purified by Ni-column (predicted weight: 54.8 kDa).

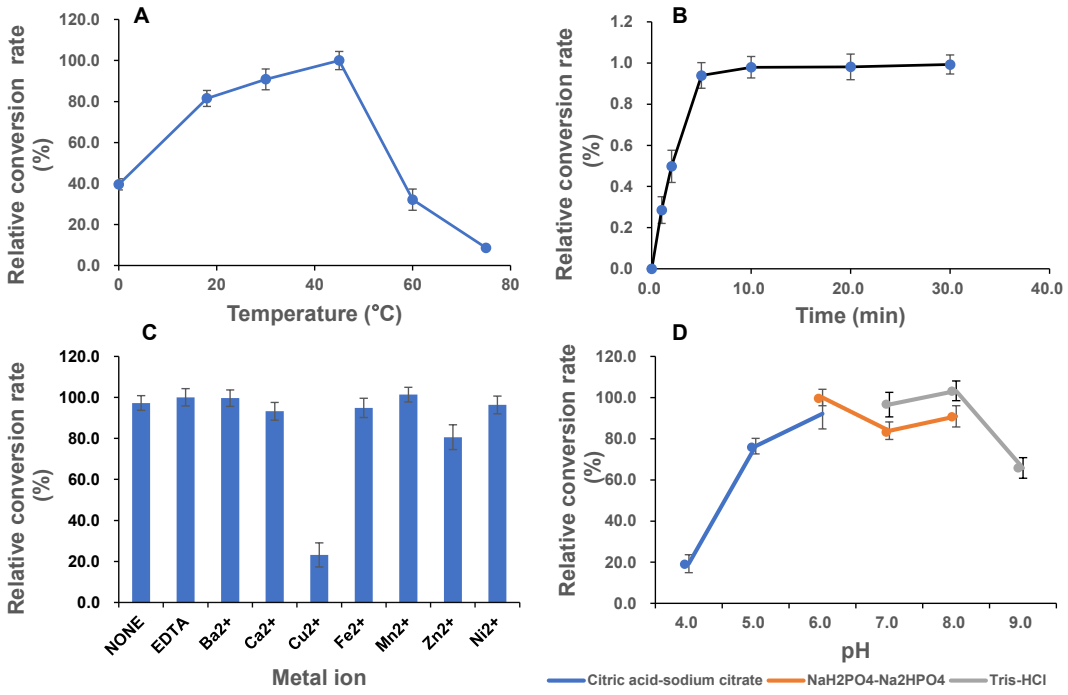

Figure S4 Optimization of the reaction temperature (A), time (B), metal ion (C) and pH (D) for AmAT19.

Cycloastragenol (**1**) was used as acyl acceptor and acetyl coenzyme A as acetyl donor. The optimized reaction condition was at pH 6.0 (50 mM NaH_2PO_4-Na_2HPO_4), incubated at 30°C for 10 min.

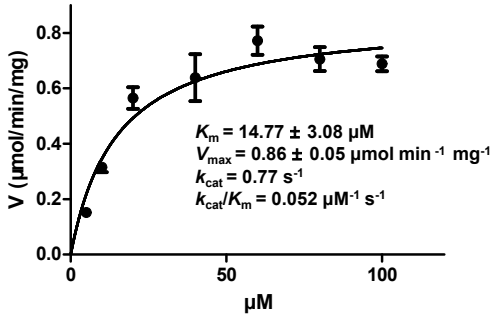

Figure S5 Kinetic analysis of AmAT19. The apparent Km value was determined using cycloastragenol (**1**) as acyl acceptor and acetyl-coenzyme A as acyl donor at 30 °C for 10 min.

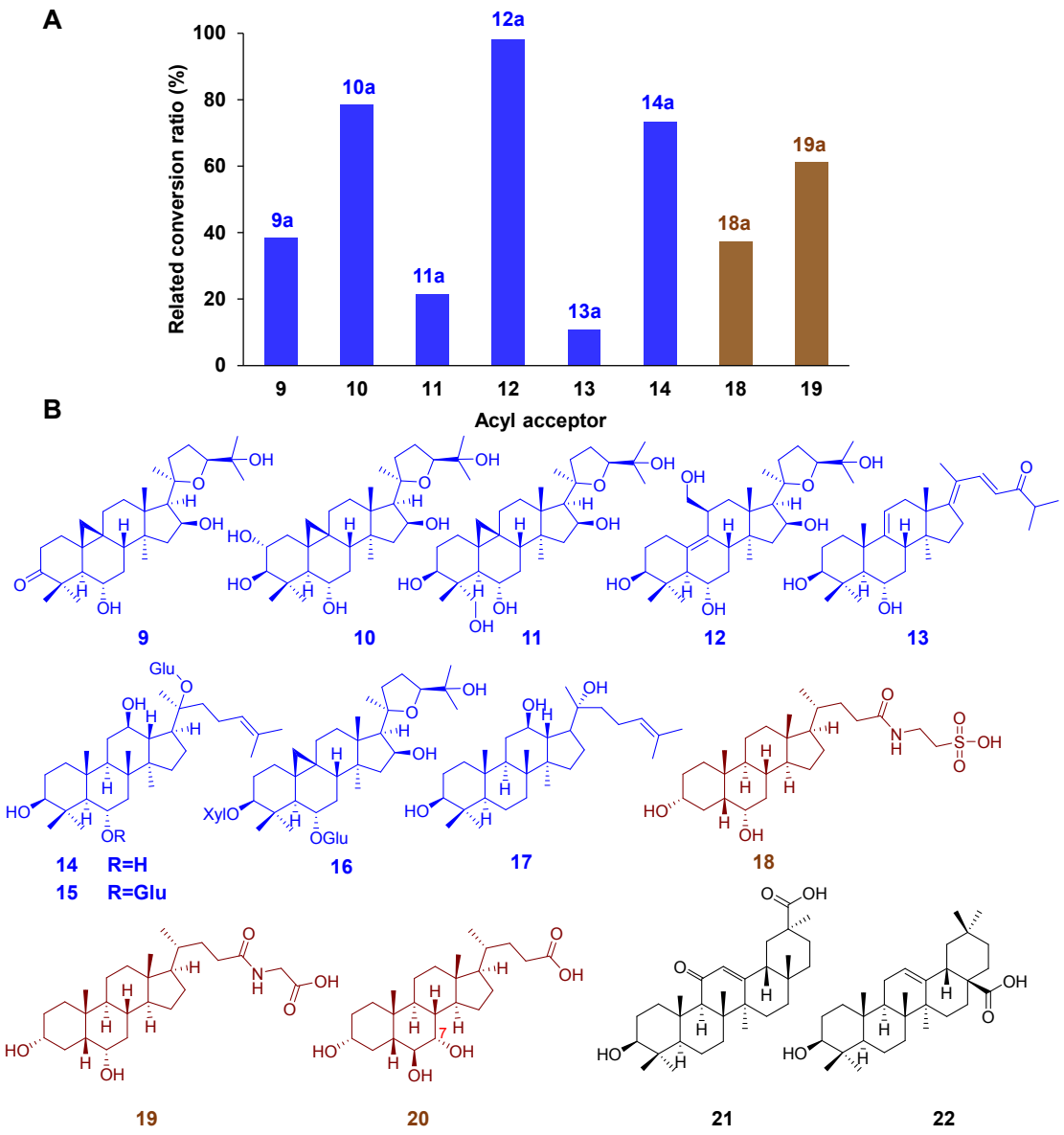

Figure S6 Substrate specificity of AmAT19

(A) Conversion rates of **9-14, 18-19** using acetyl-CoA as the acyl donor. (B) Structures of acetyl acceptors **9**–**22**. Compound **9-14, 18-19** could be acetylated by AmAT19, which was characterized by MS spectra.

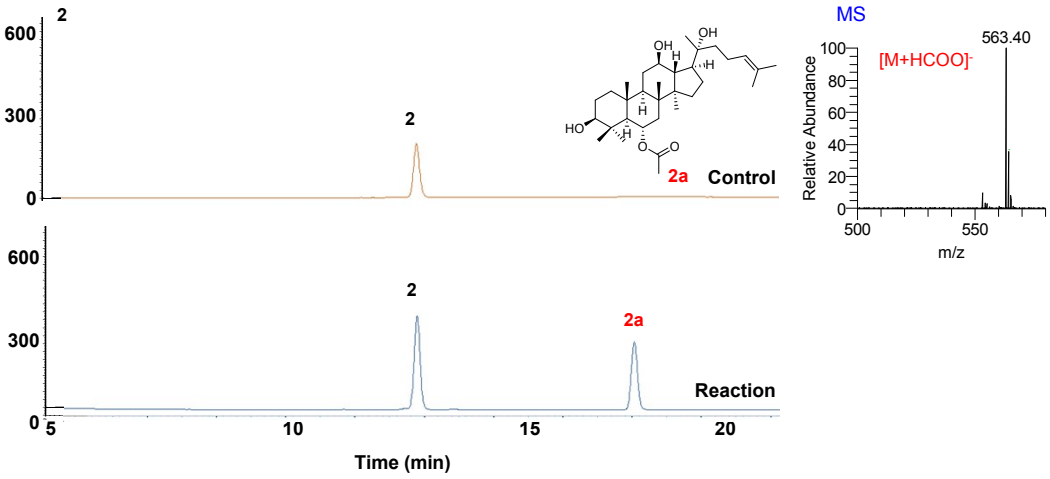

Figure S7 HPLC/ELSD chromatograms of the reaction mixtures for AmAT19 using **2** as the acyl acceptor, and the MS spectra of product **2a**.

Reaction, acetyl-CoA was added as the acyl donor; control, the acyl donor is absent. MS spectra of **2a** were obtained in negative ion mode. The MS/MS spectra is not available due to the poor fragmentation of the $[M+HCOO]^-$ adduct ion.

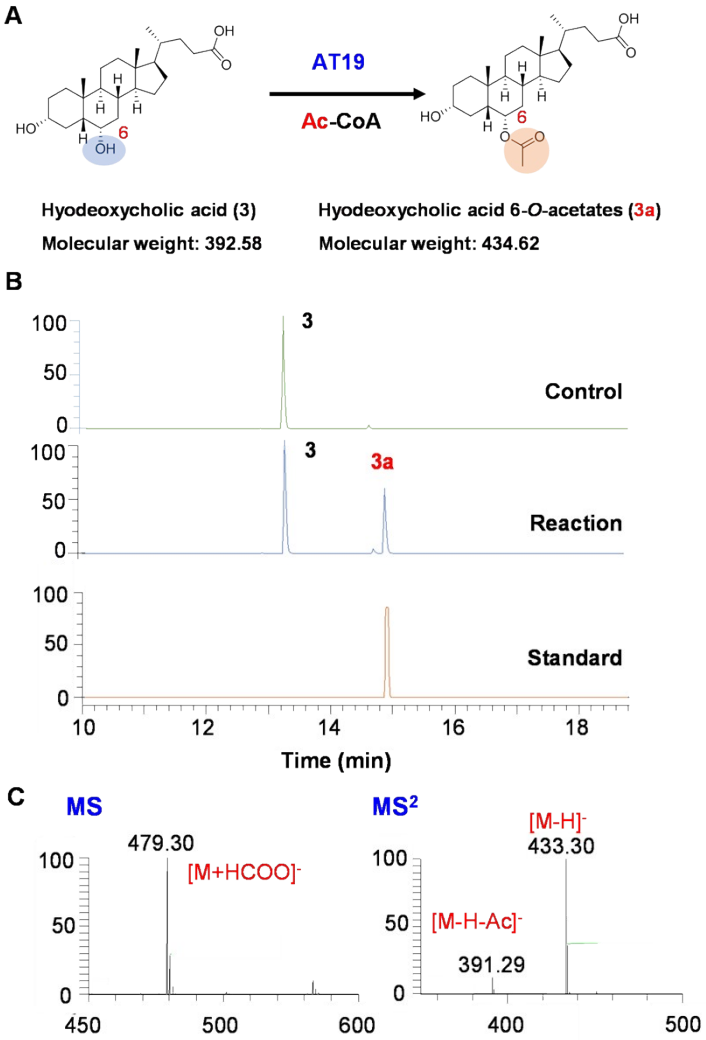

Figure S8 UHPLC/MS chromatograms of the reaction mixtures for AmAT19 using **3** as the acyl acceptor, and the MS spectra of product **3a**.

(A) Acylation of hyodeoxycholic acid (**3**) catalyzed by AmAT19. (B) UHPLC/MS extracted ion chromatograms (*m*/*z* 479.3 and 437.3) of the control, reaction and the reference standard samples. (C) HR-MS and HR-MS/MS spectra of the product **3a** in negative ion mode.

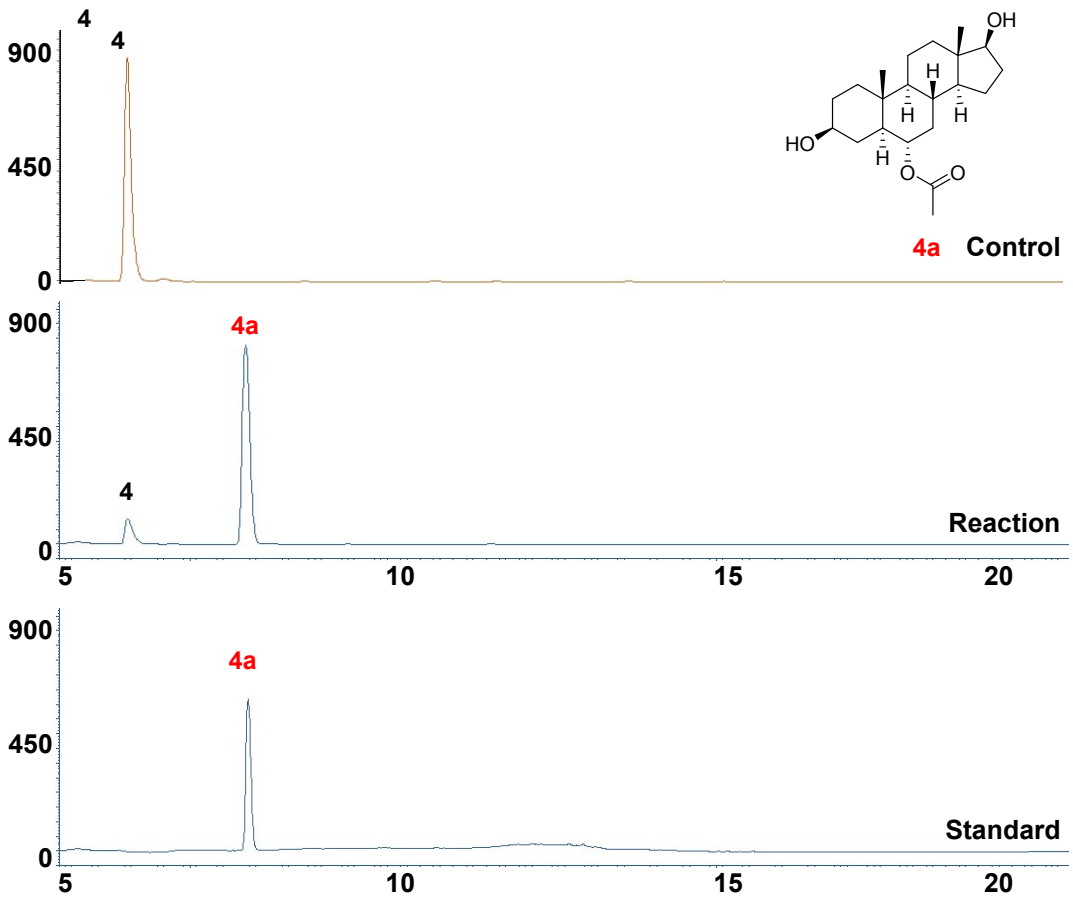

Figure S9 HPLC/ELSD chromatograms of the reaction mixtures for AmAT19 using **4** as the acyl acceptor.

Reaction, acetyl-CoA was added as the acyl donor; control, the acyl donor is absent. The mass spectrometry data of **4a** was not available due to poor ionization. The structure of **4a** was further confirmed by NMR.

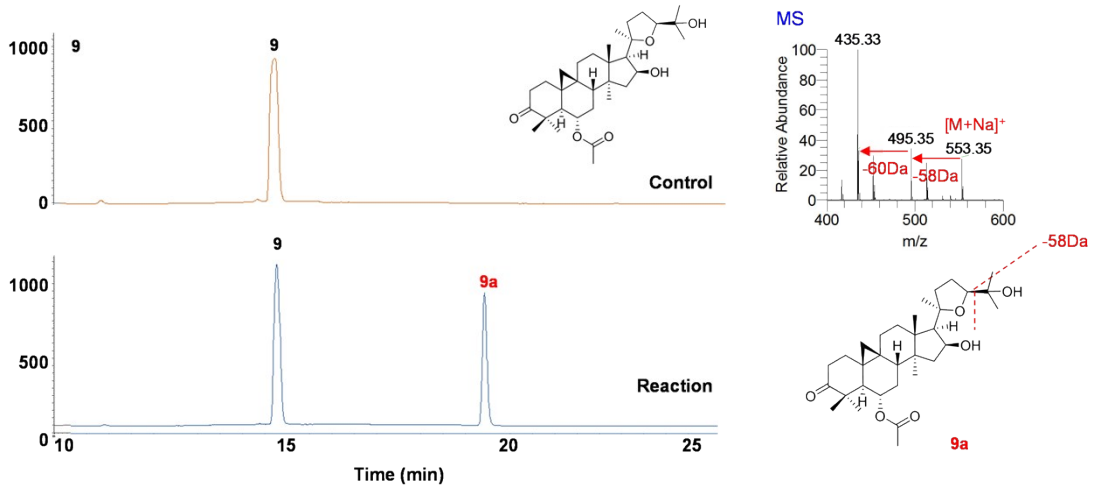

Figure S10 HPLC/ELSD chromatograms of the reaction mixtures for AmAT19 using **9** as the acyl acceptor, and the MS spectra of product **9a**.

Reaction, acetyl-CoA was added as the acyl donor; control, the acyl donor is absent. MS spectra of **9a** was obtained in positive ion mode, and the fragments could be observed due to in-source fragmentation. The mass difference of 60 Da and 58 Da indicated the acetic acid and the side chain, respectively.

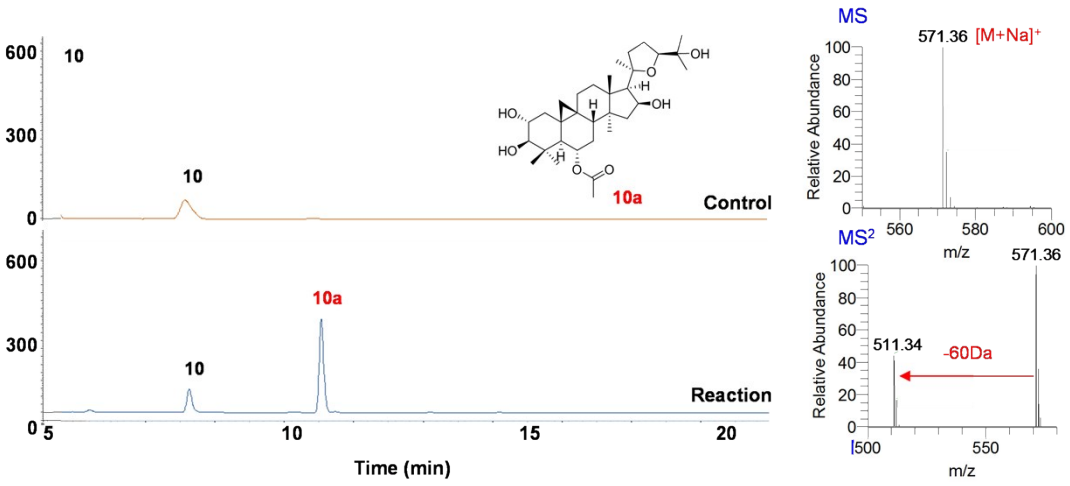

Figure S11 HPLC/ELSD chromatograms of the reaction mixtures for AmAT19 using **10** as the acyl acceptor, and the MS and MS/MS spectra of product **10a**.

Reaction, acetyl-CoA was added as the acyl donor; control, the acyl donor is absent. MS and MS/MS spectra of **10a** were obtained in positive ion mode. The mass difference of 60 Da indicated the acetic acid.

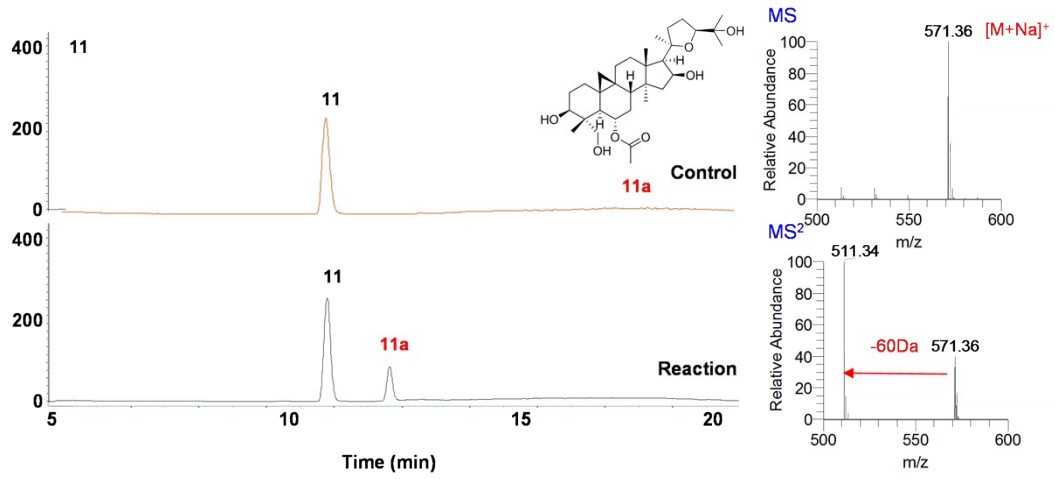

Figure S12 HPLC/ELSD chromatograms of the reaction mixtures for AmAT19 using **11** as the acyl acceptor, and the MS and MS/MS spectra of product **11a**.

Reaction, acetyl-CoA was added as the acyl donor; control, the acyl donor is absent. MS and MS/MS spectra of **11a** were obtained in positive ion mode. The mass difference of 60 Da indicated the acetic acid.

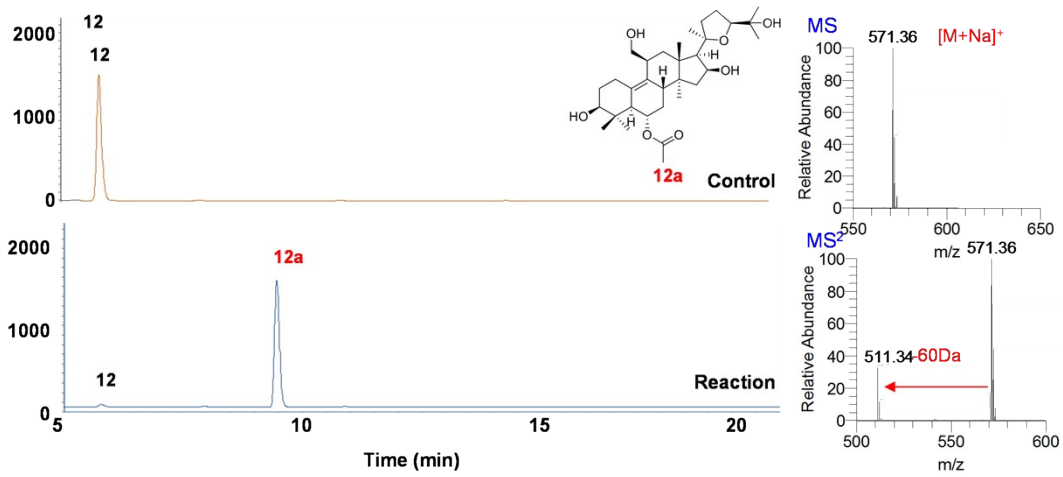

Figure S13 HPLC/ELSD chromatograms of the reaction mixtures for AmAT19 using **12** as the acyl acceptor, and the MS and MS/MS spectra of product **12a**.

Reaction, acetyl-CoA was added as the acyl donor; control, the acyl donor is absent. MS and MS/MS spectra of **12a** were obtained in positive ion mode. The mass difference of 60 Da indicated the acetic acid.

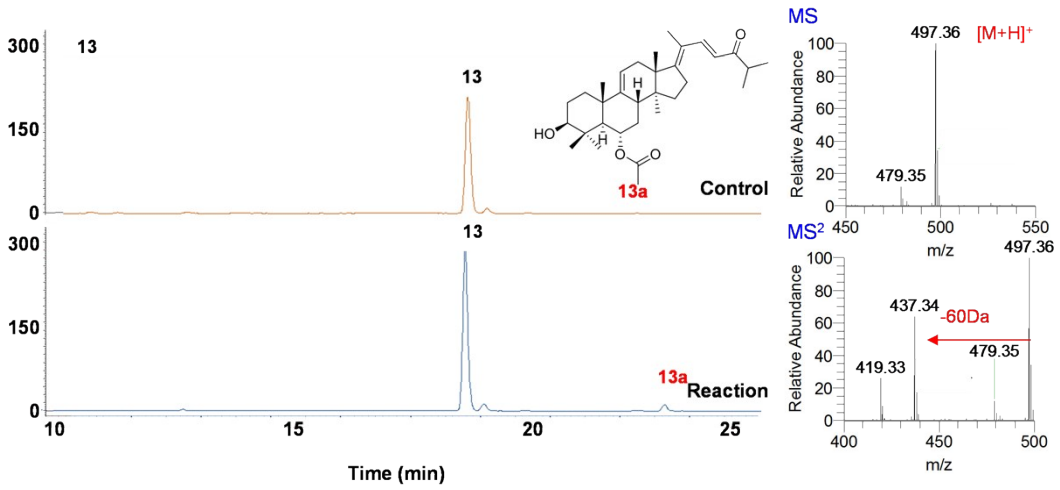

Figure S14 HPLC/ELSD chromatograms of the reaction mixtures for AmAT19 using **13** as the acyl acceptor, and the MS and MS/MS spectra of product **13a**.

Reaction, acetyl-CoA was added as the acyl donor; control, the acyl donor is absent. MS and MS/MS spectra of **13a** were obtained in positive ion mode. The mass difference of 60 Da indicated the acetic acid.

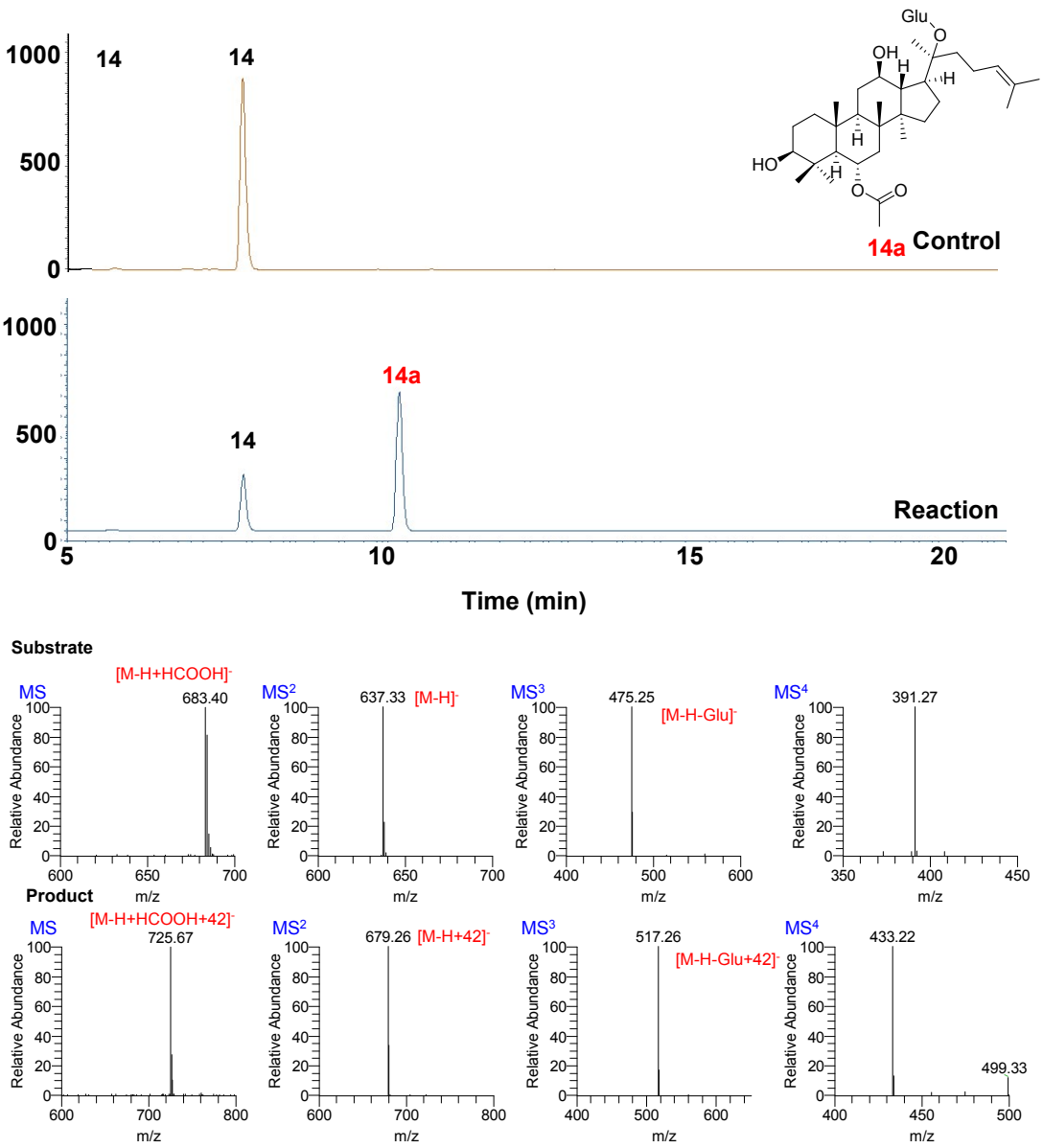

Figure S15 HPLC/ELSD chromatograms of the reaction mixtures for AmAT19 using **14** as the acyl acceptor, and the MS and MS/MS spectra of product **14** and **14a**. Reaction, acetyl-CoA was added as the acyl donor; control, the acyl donor is absent. MS and MS^n spectra of **14** and **14a** were obtained in negative ion mode using an ion trap mass spectrometer (LCQ Advantage, Thermo Finnigan, USA). The mass difference between **14** and **14a** and their fragments maintained 42 Da (acetyl group) in MS^n analysis.

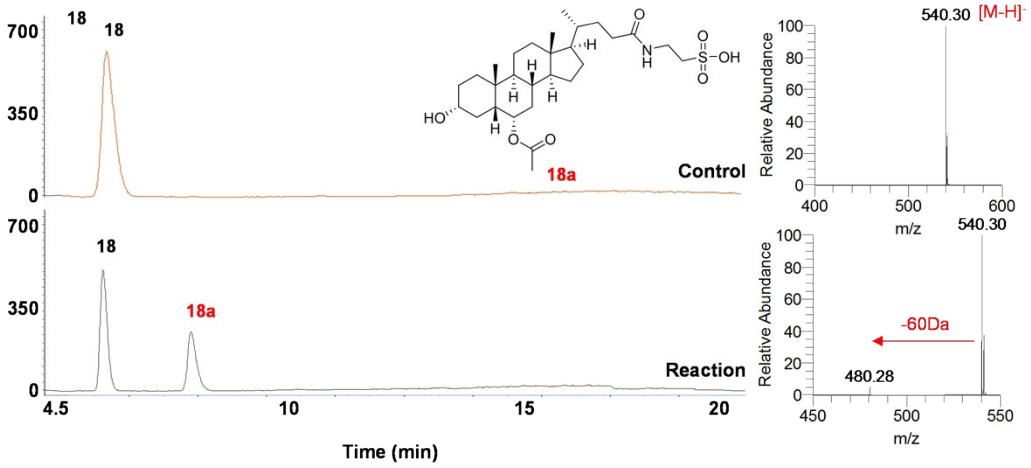

Figure S16 HPLC/ELSD chromatograms of the reaction mixtures for AmAT19 using **18** as the acyl acceptor, and the MS and MS/MS spectra of product **18a**.

Reaction, acetyl-CoA was added as the acyl donor; control, the acyl donor is absent. MS and MS/MS spectra of **18a** were obtained in positive ion mode. The mass difference of 60 Da indicated the acetic acid.

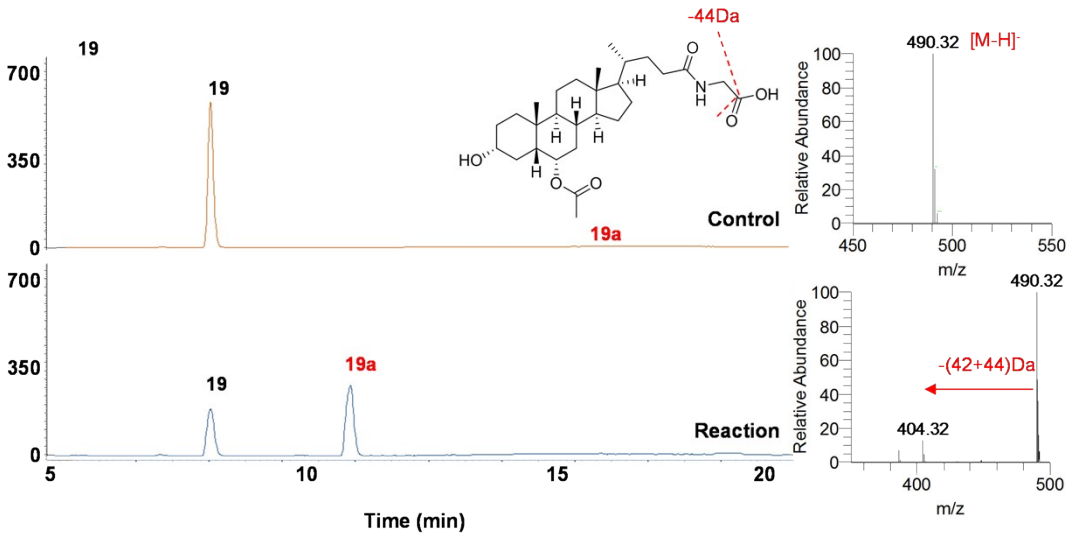

Figure S17 HPLC/ELSD chromatograms of the reaction mixtures for AmAT19 using **19** as the acyl acceptor, and the MS and MS/MS spectra of product **19a**.

Reaction, acetyl-CoA was added as the acyl donor; control, the acyl donor is absent. MS and MS/MS spectra of **19a** were obtained in negative ion mode. The neutral loss of 42+44 Da indicated the acetyl and the carboxyl groups.

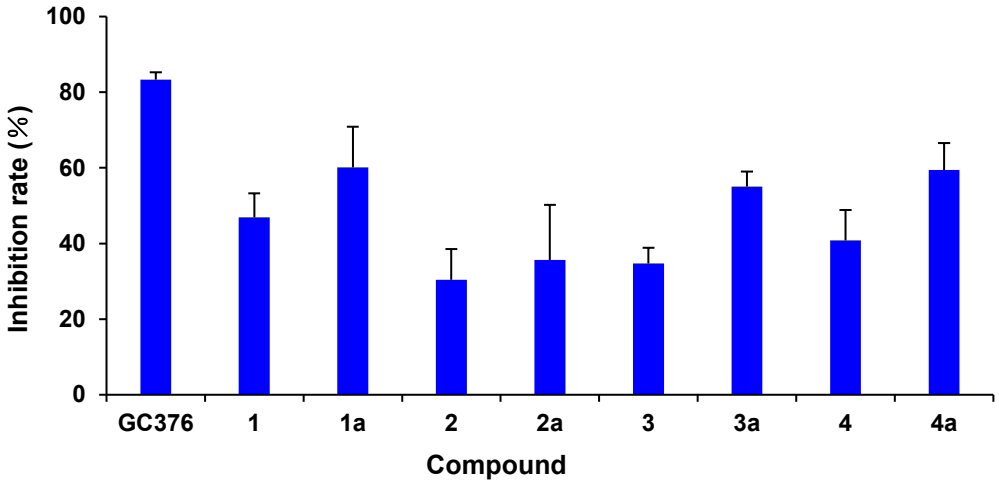

Figure S18 3CL^{pro} inhibition activity for **1**/**1a**, **2**/**2a, 3**/**3a and 4**/**4a** at 8 μM. GC376 was a positive control applied from a previous study [4].

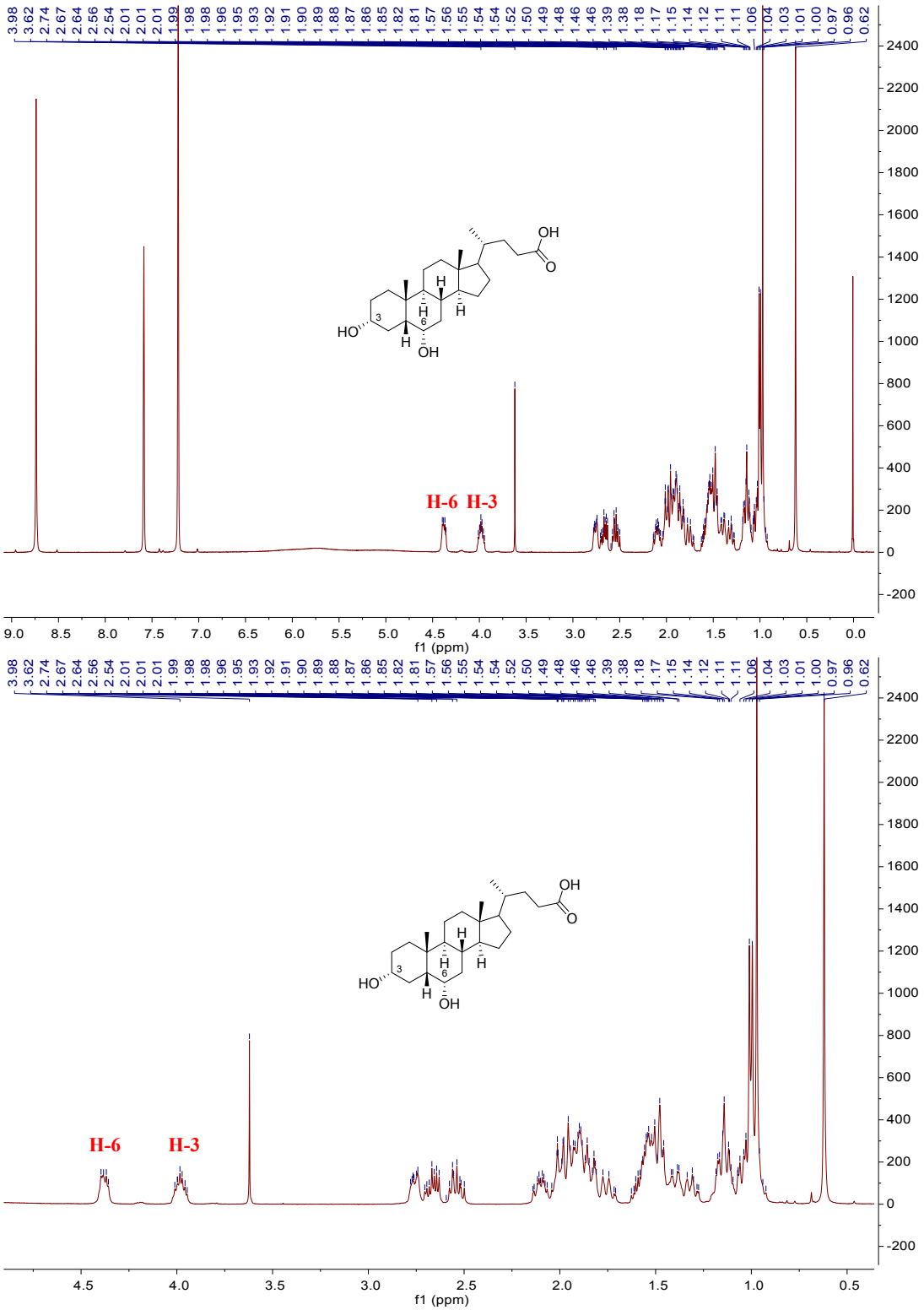

Figure S19 ^{1}H NMR spectrum of **3** in pyridine-d_5 (400 MHz).

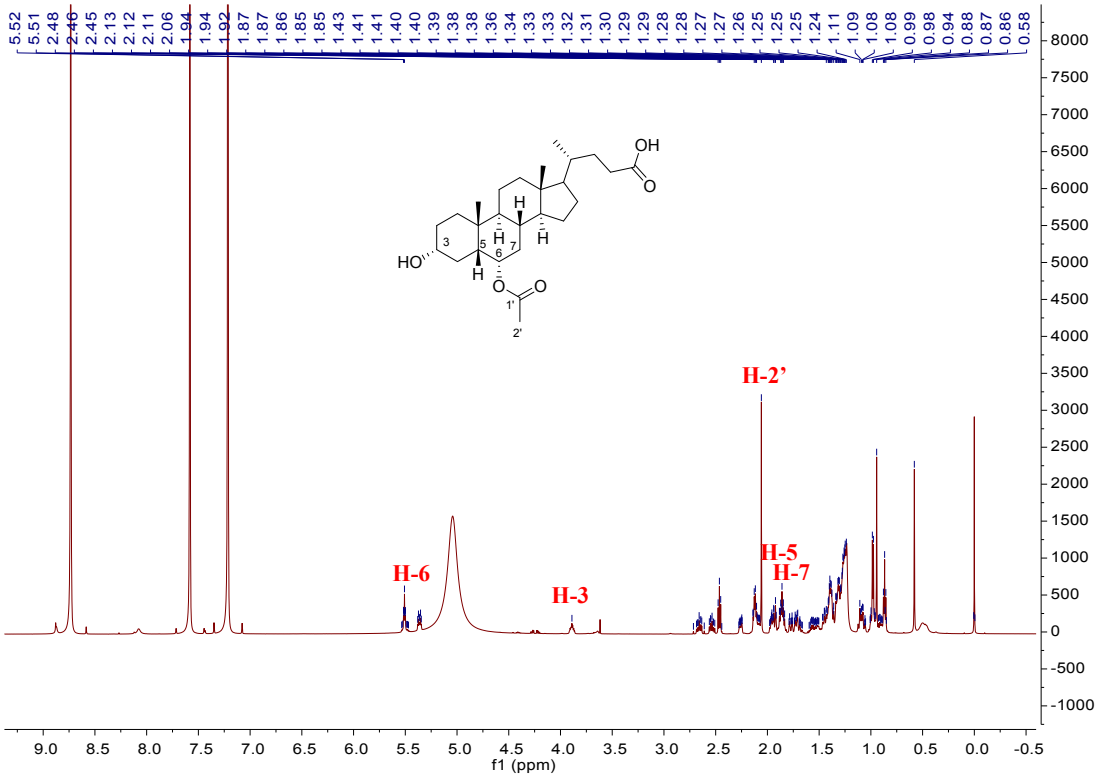

Figure S20 ^{1}H NMR spectrum of **3a** in pyridine-d_5 (600 MHz).

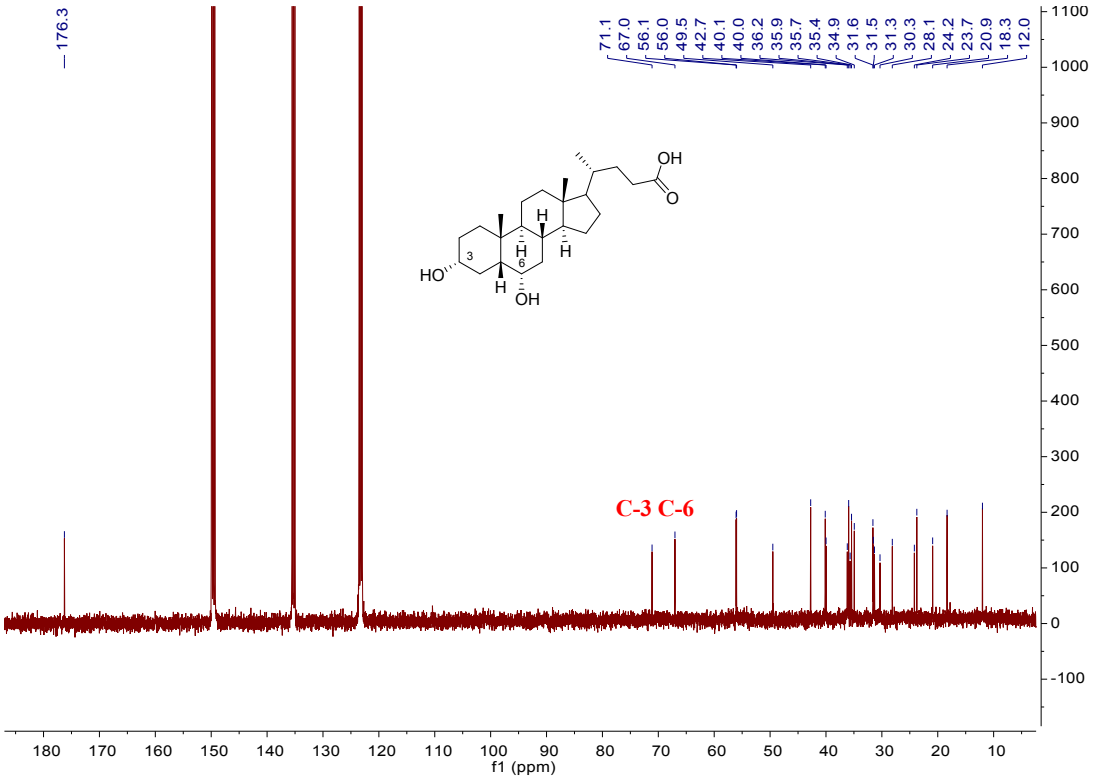

Figure S21 ^{13}C NMR spectrum of **3** in pyridine-d_5 (400 MHz).

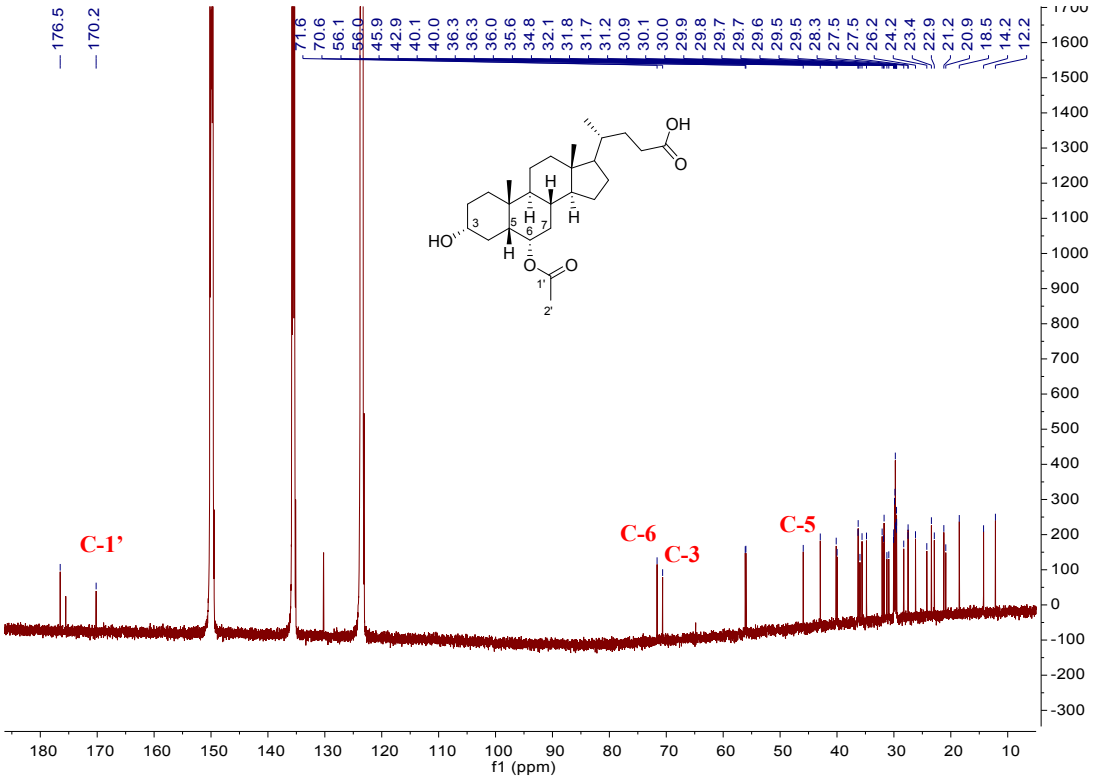

Figure S22 ^{13}C NMR spectrum of **3a** in pyridine-d_5 (600 MHz).

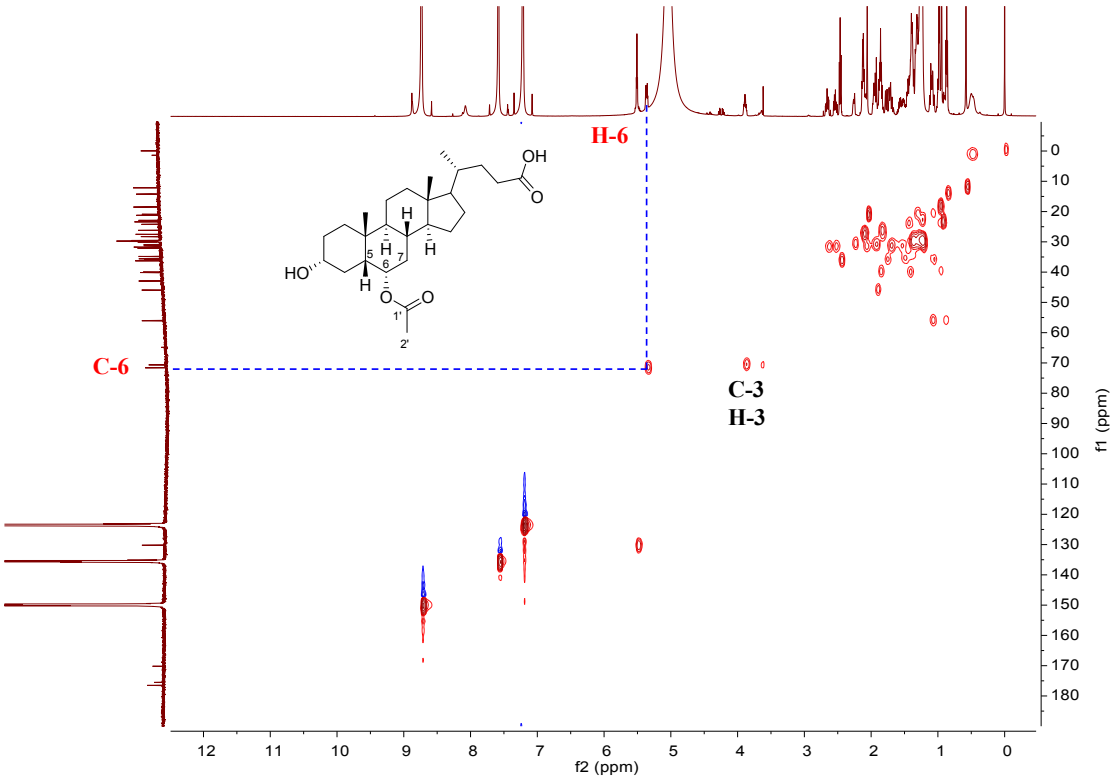

Figure S23 HSQC spectrum of **3a** in pyridine-d_5 (400 MHz).

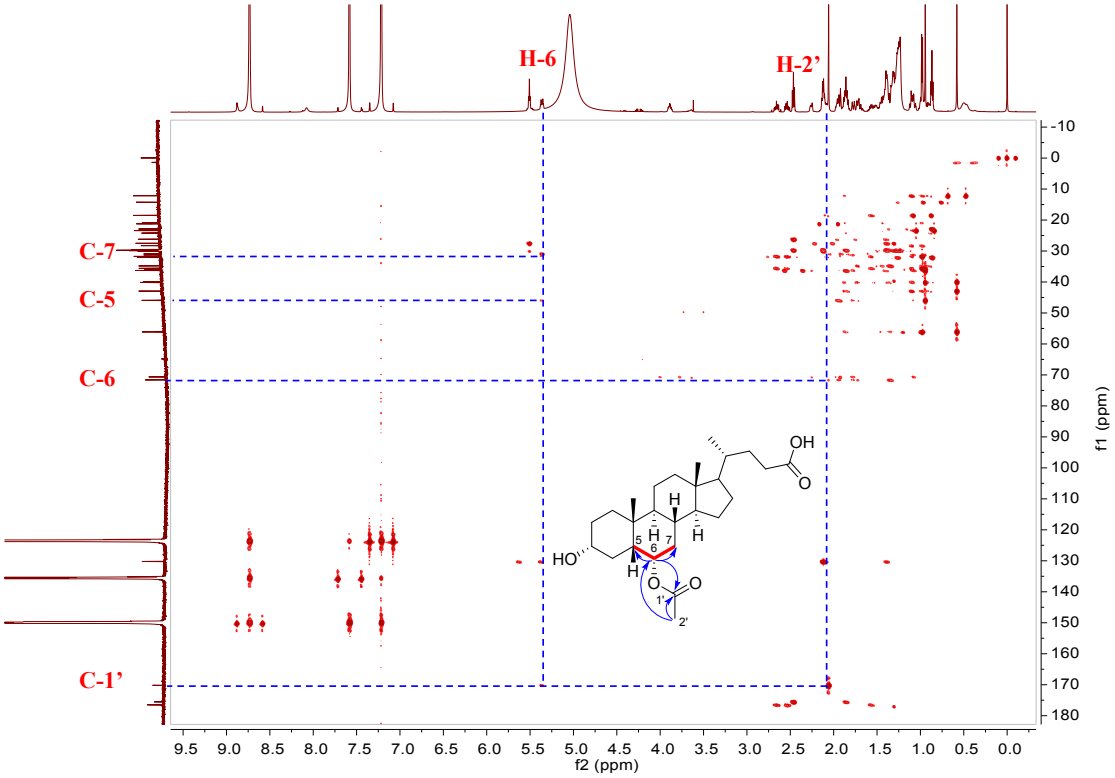

Figure S24 HMBC spectrum of **3a** in pyridine-d_5 (600 MHz).

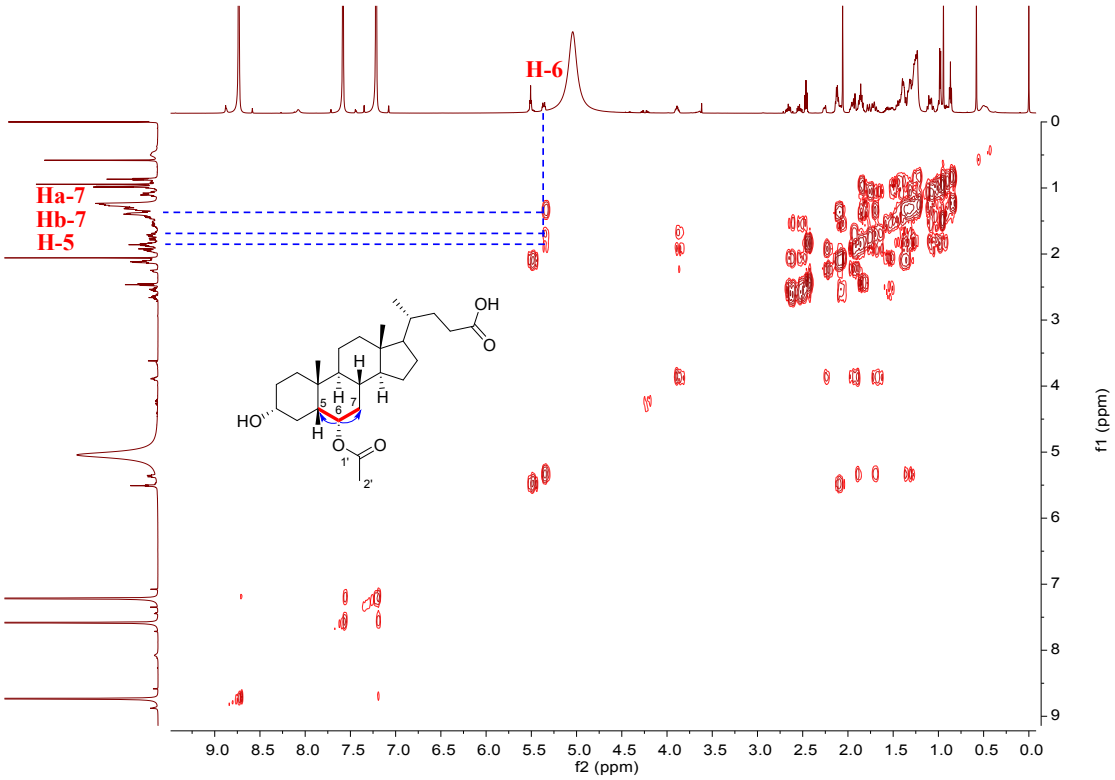

Figure S25 ^{1}H-^{1}H-COSY spectrum of **3a** in pyridine-d_5 (400 MHz).

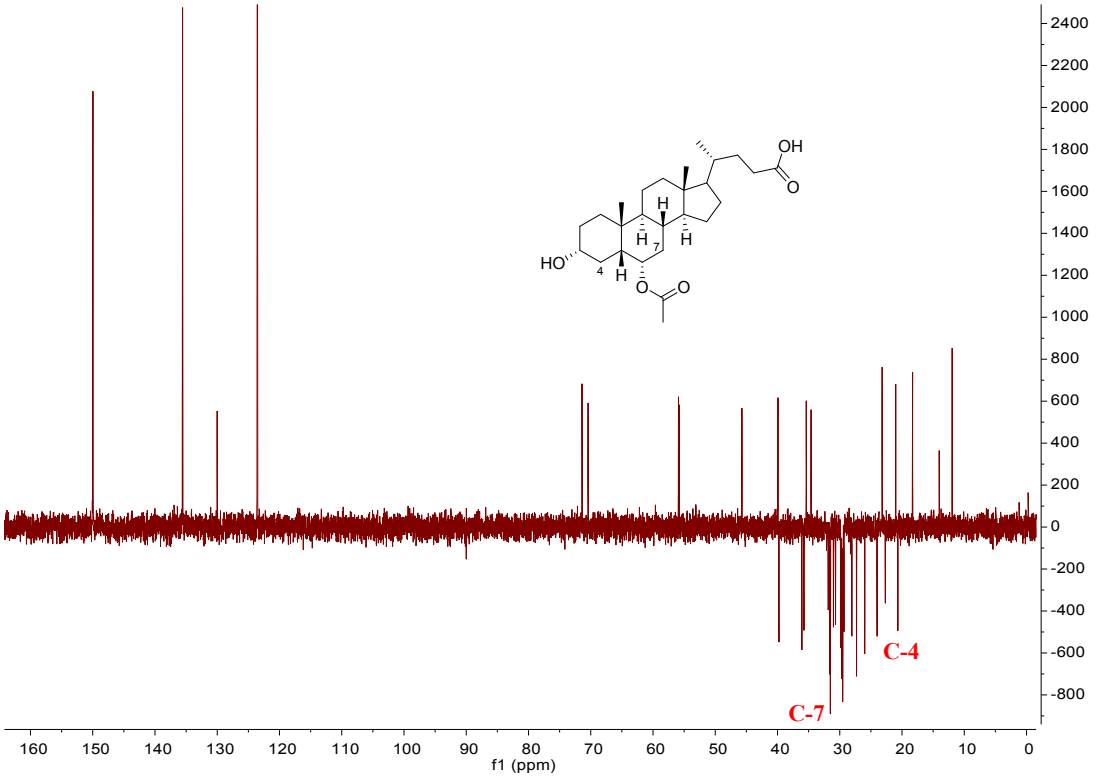

Figure S26DEPT135 spectrum of **14a** in pyridine-d_5 (400 MHz).

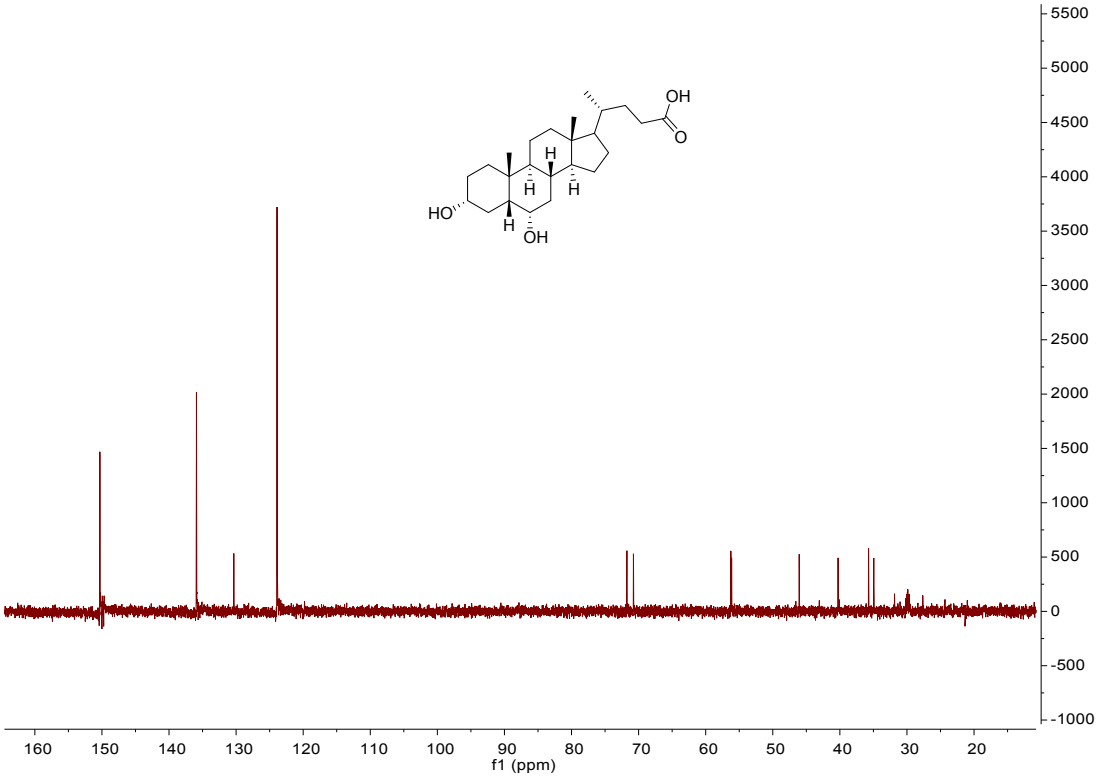

Figure S27 DEPT90 spectrum of **3a** in pyridine-d_5 (400 MHz).

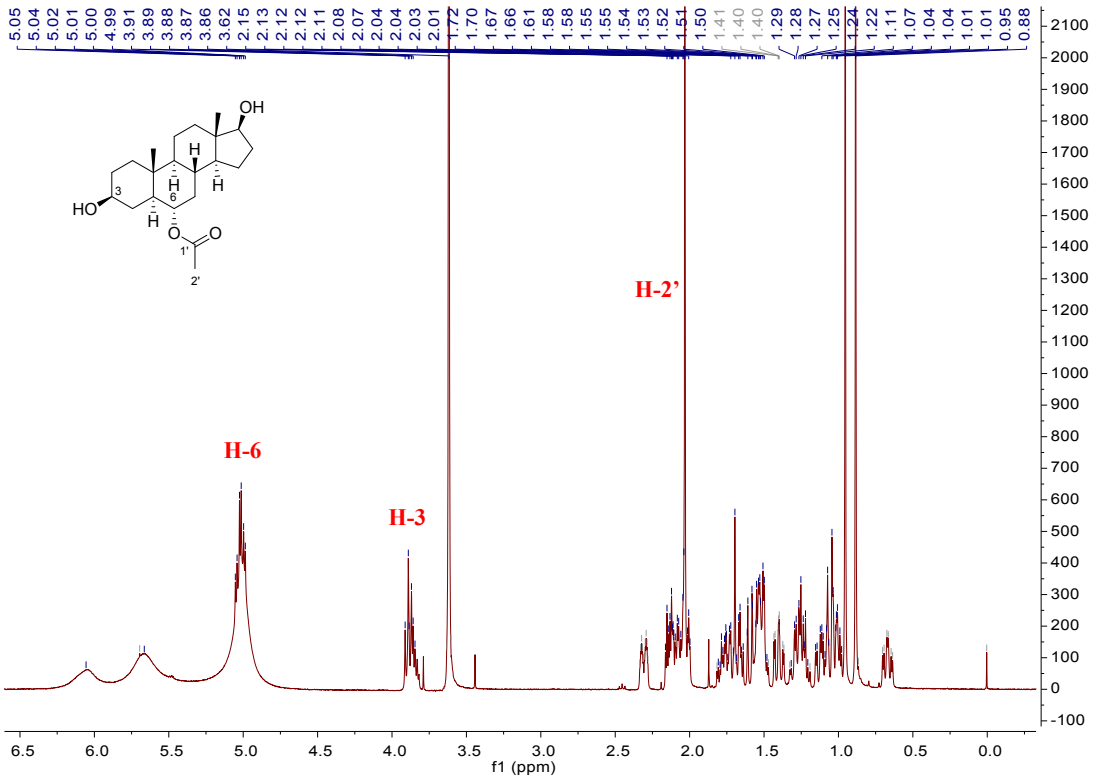

Figure S28 ^{1}H NMR spectrum of **4a** in pyridine-d_5 (400 MHz).

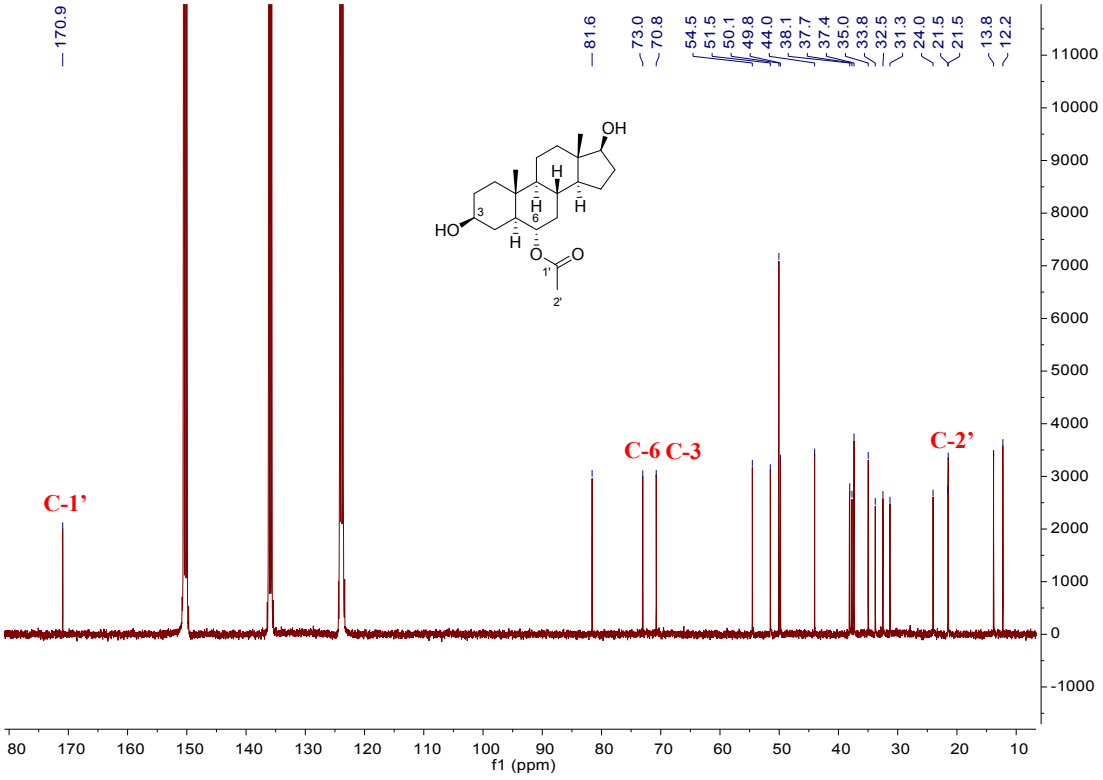

Figure S29 ^{13}C NMR spectrum of **4a** in pyridine-d_5 (400 MHz).

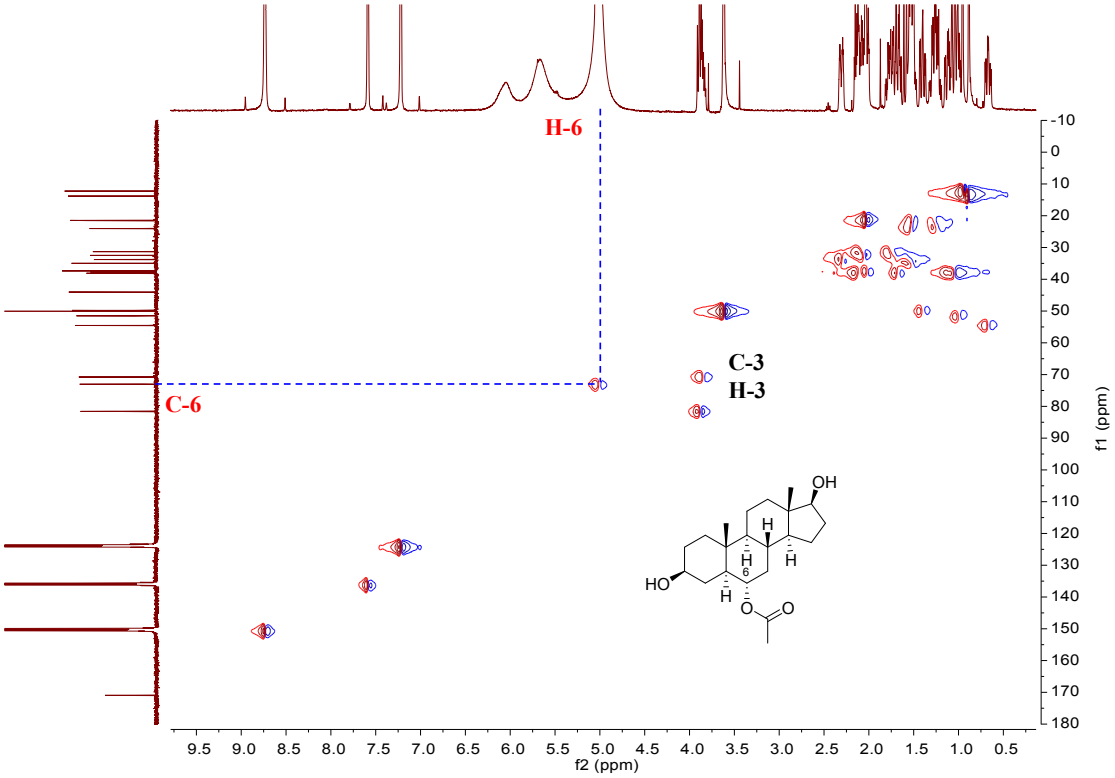

Figure S30 HSQC spectrum of **4a** in pyridine-d_5 (400 MHz).

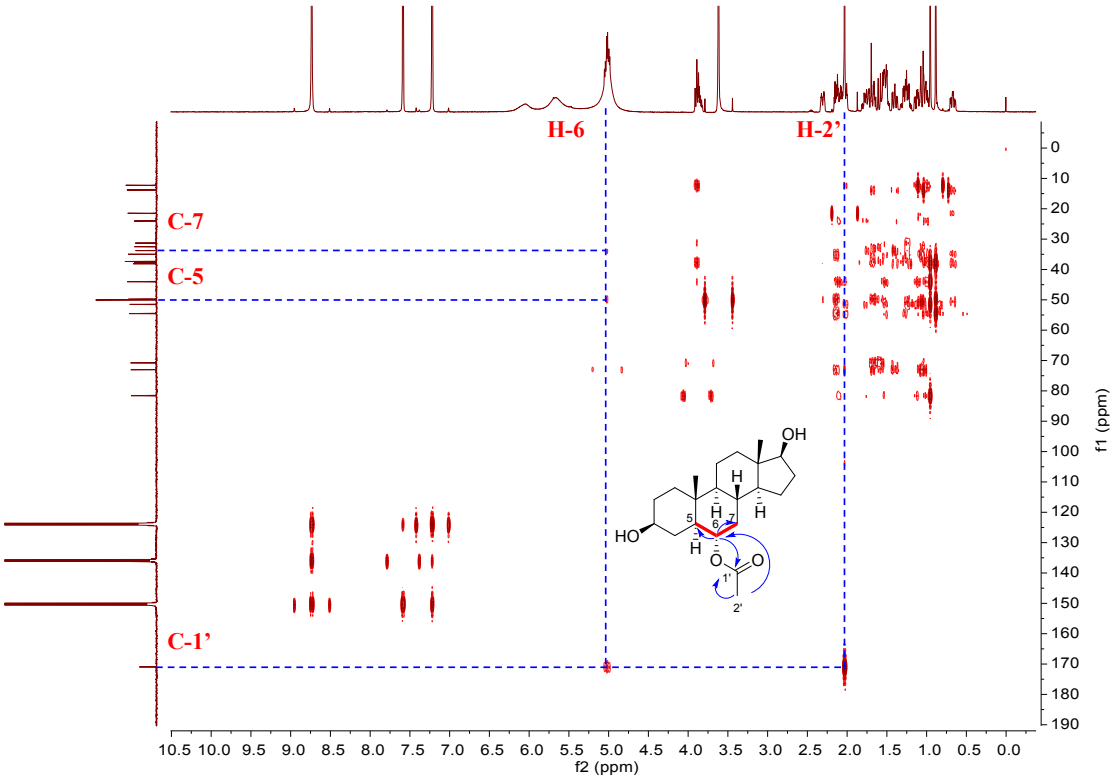

Figure S31 HMBC spectrum of **4a** in pyridine-d_5 (400 MHz).

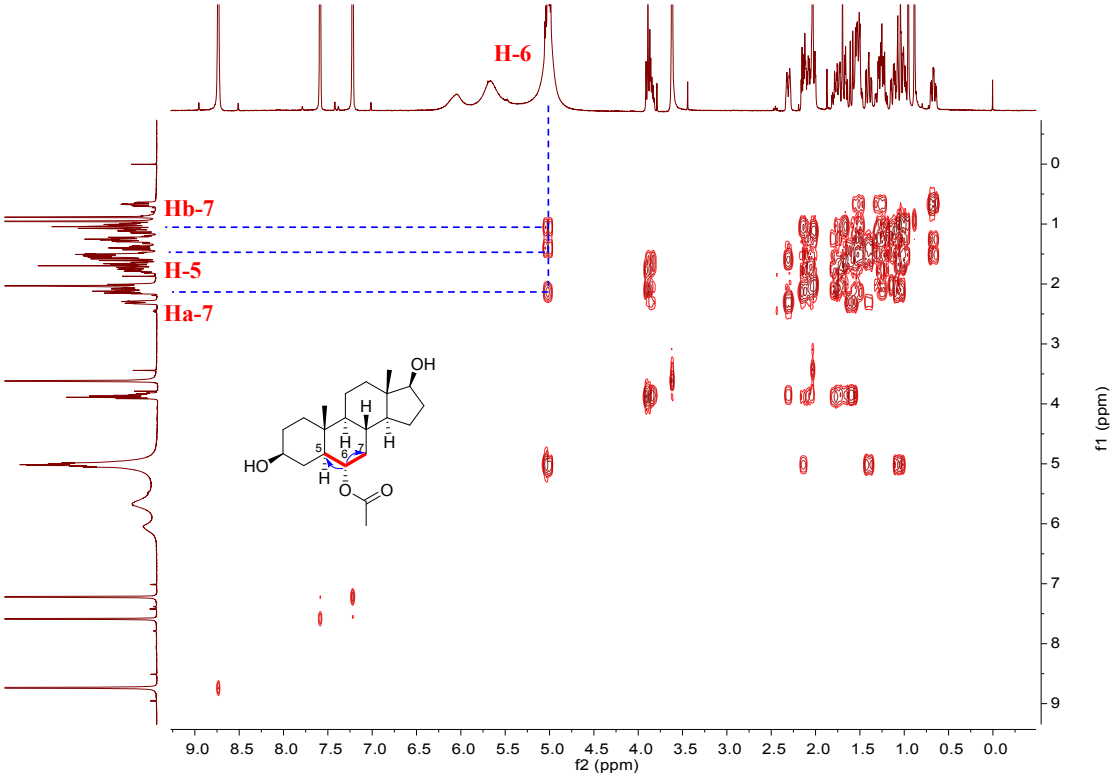

Figure S32 ^{1}H-^{1}H COSY spectrum of **4a** in pyridine-d_5 (400 MHz).

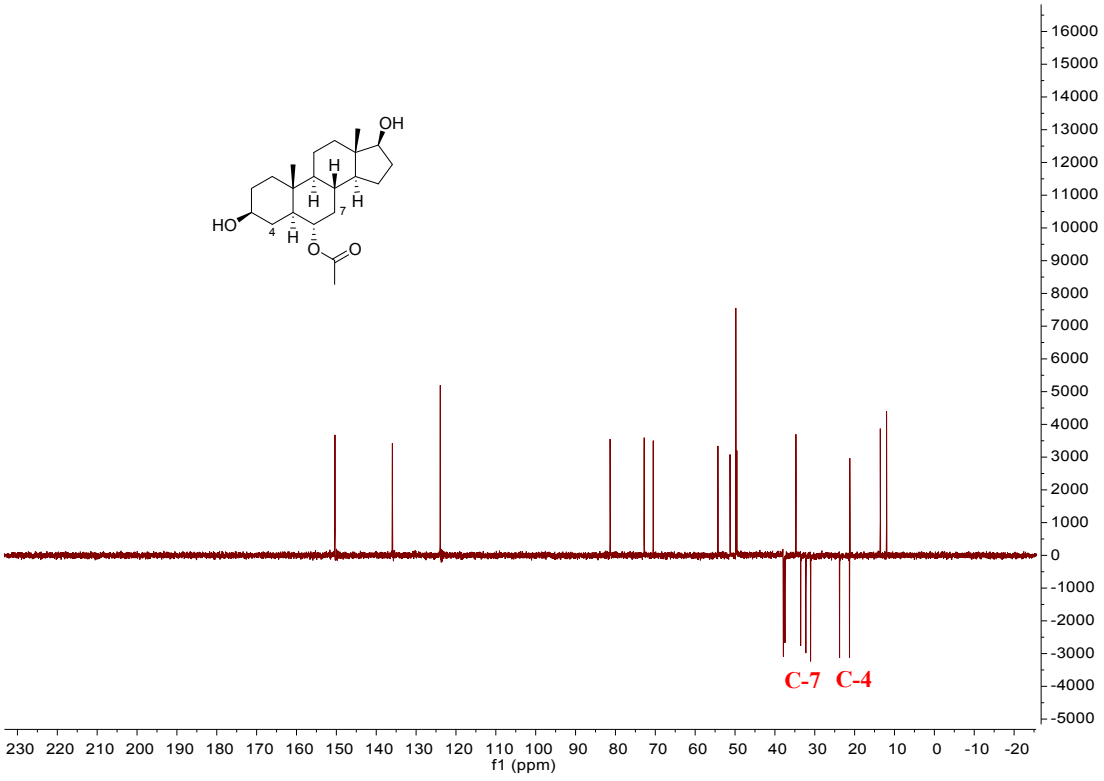

Figure S33 DEPT 135 spectrum of **4a** in pyridine-d_5 (400 MHz).

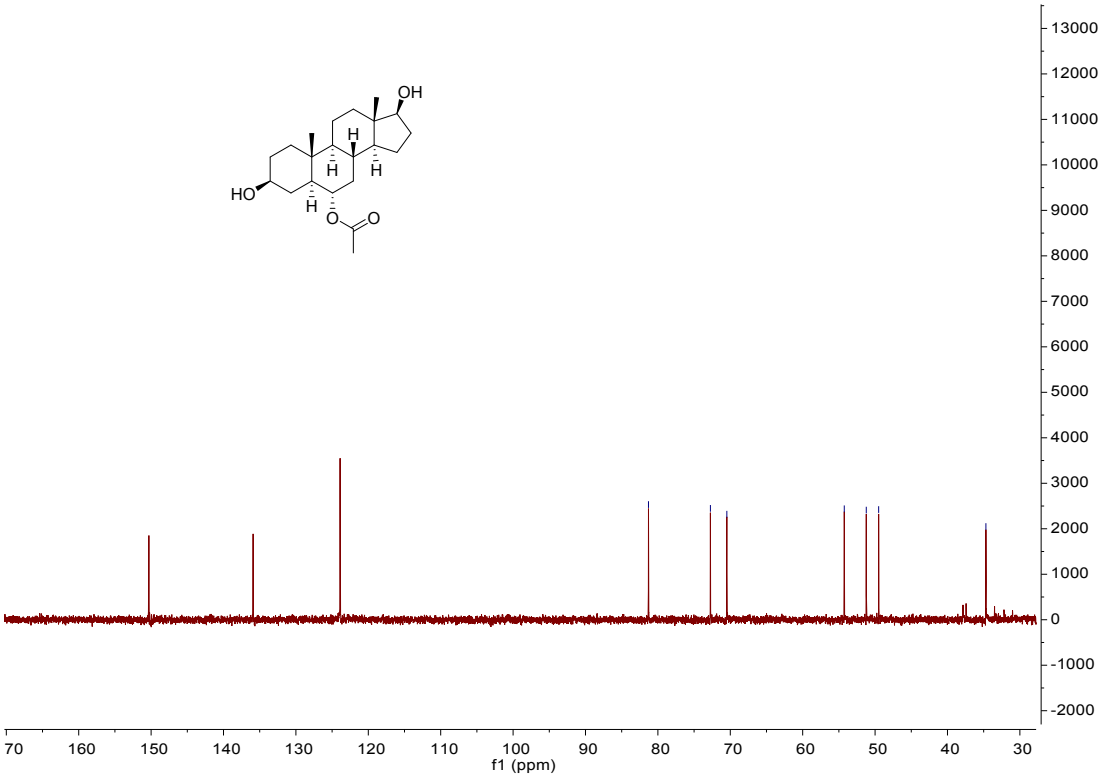

Figure S34 DEPT 90 spectrum of **4a** in pyridine-d_5 (400 MHz).

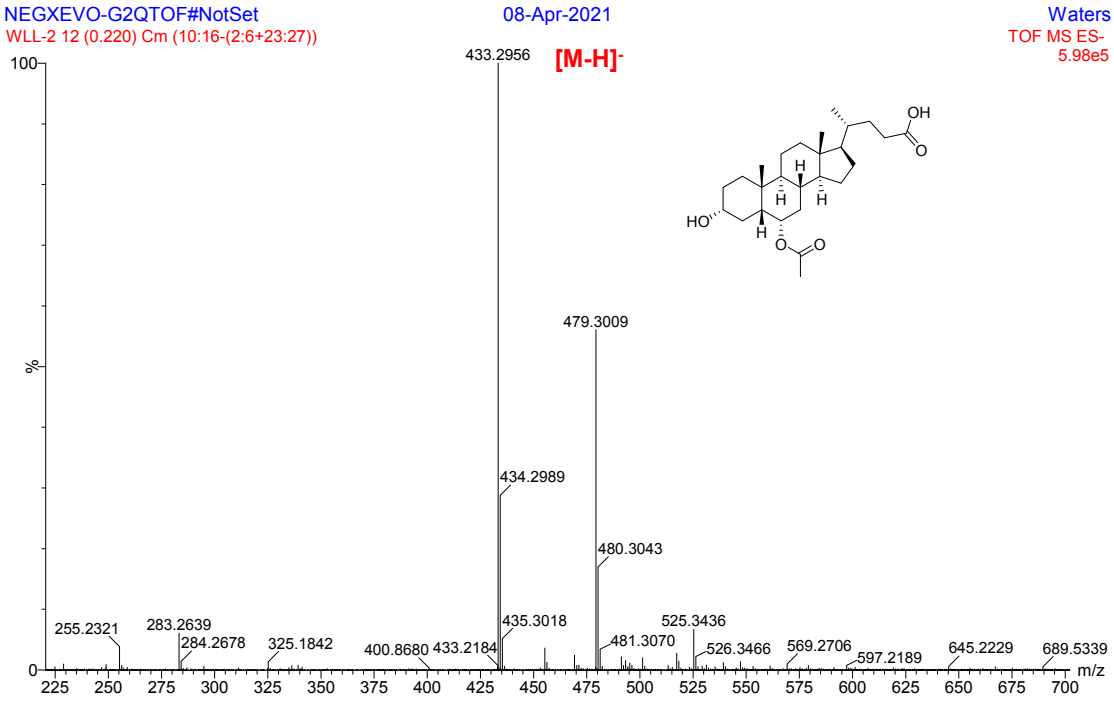

Figure S35 (-)ESI-HR-MS spectrum of **3a**.

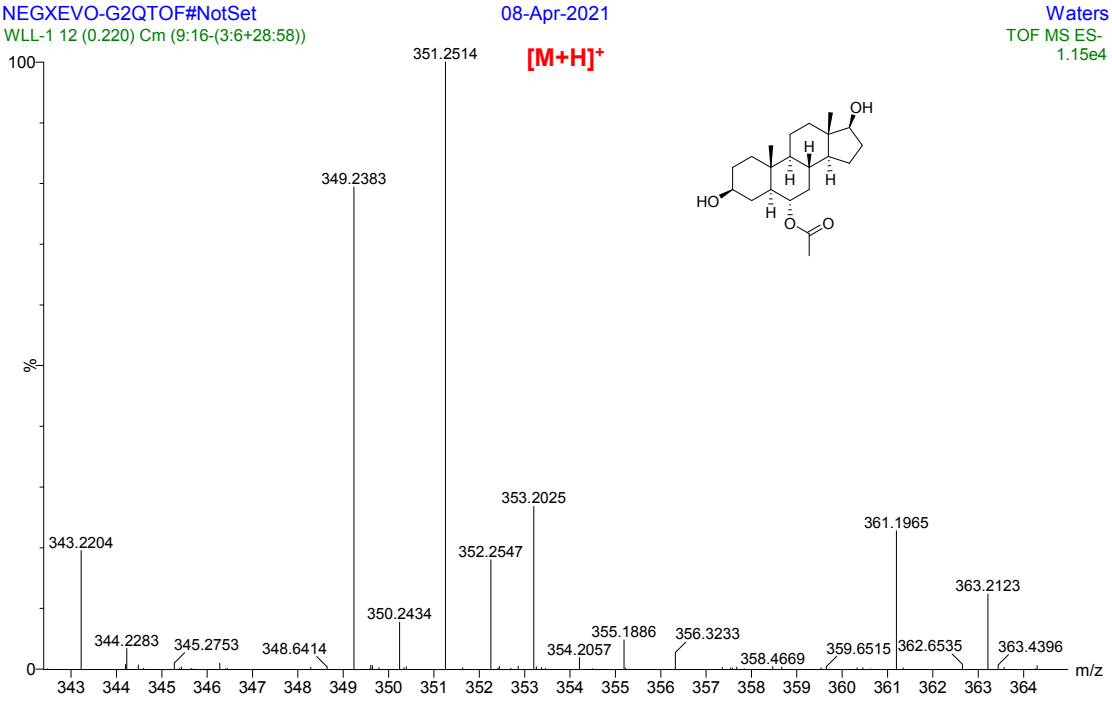

Figure S36 (-)ESI-HR-MS spectrum of **4a**.

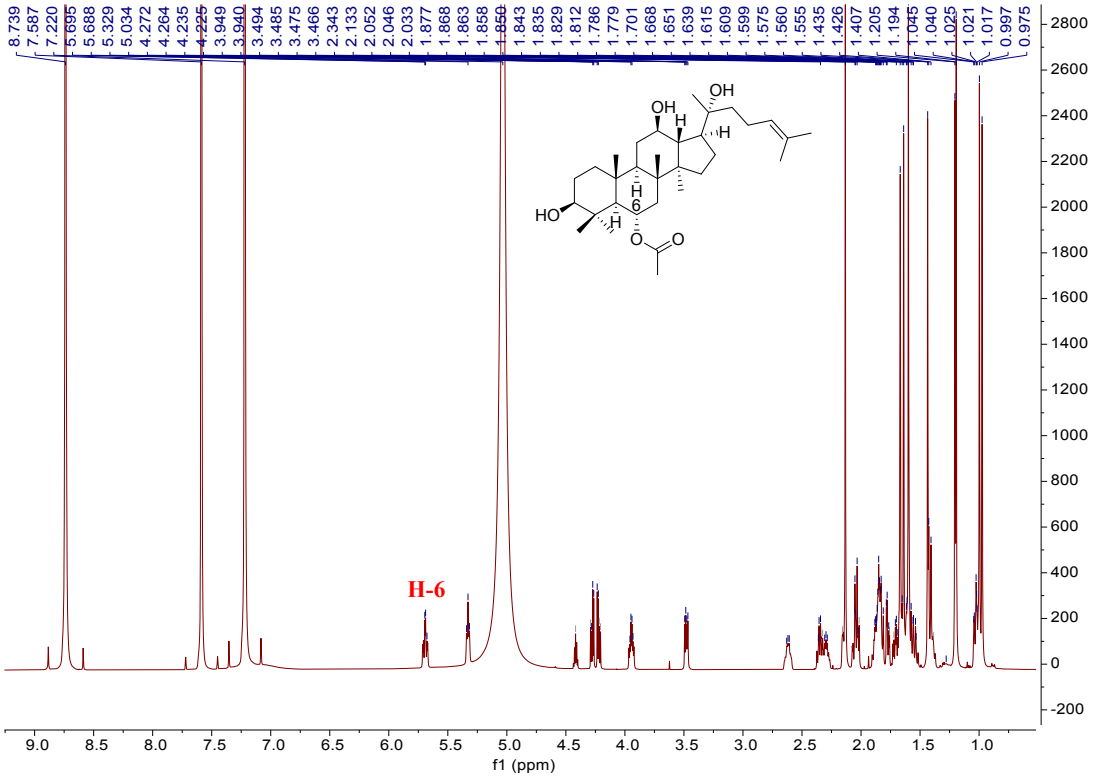

Figure S37 ^{1}H NMR spectrum of **2a** in pyridine-d_5 (600 MHz).

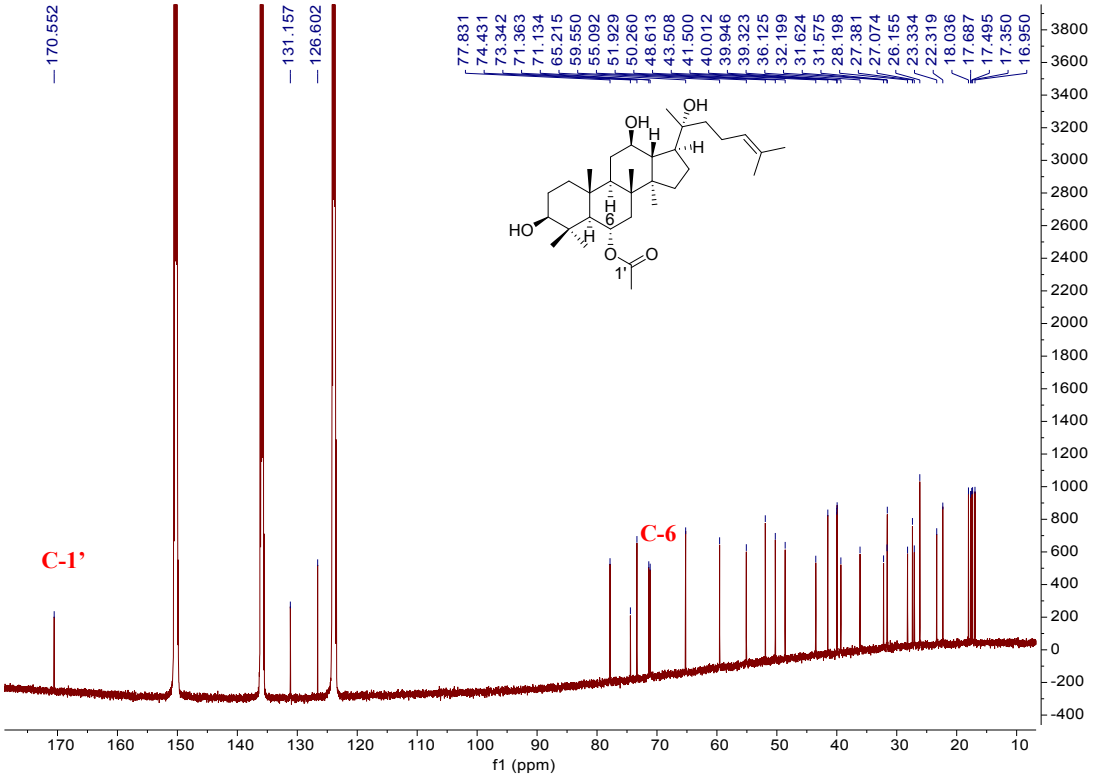

Figure S38 ^{13}C NMR spectrum of **2a** in pyridine-d_5 (600 MHz).

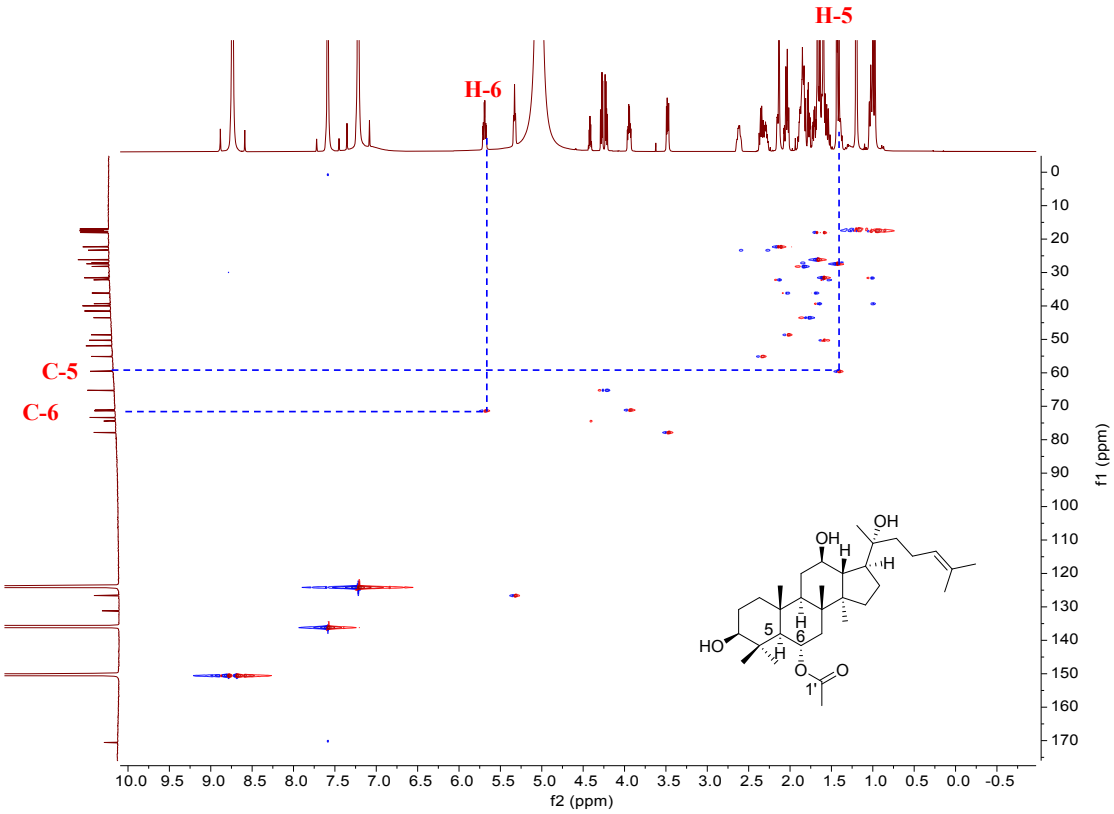

Figure S39 HSQC spectrum of **2a** in pyridine-d_5 (600 MHz).

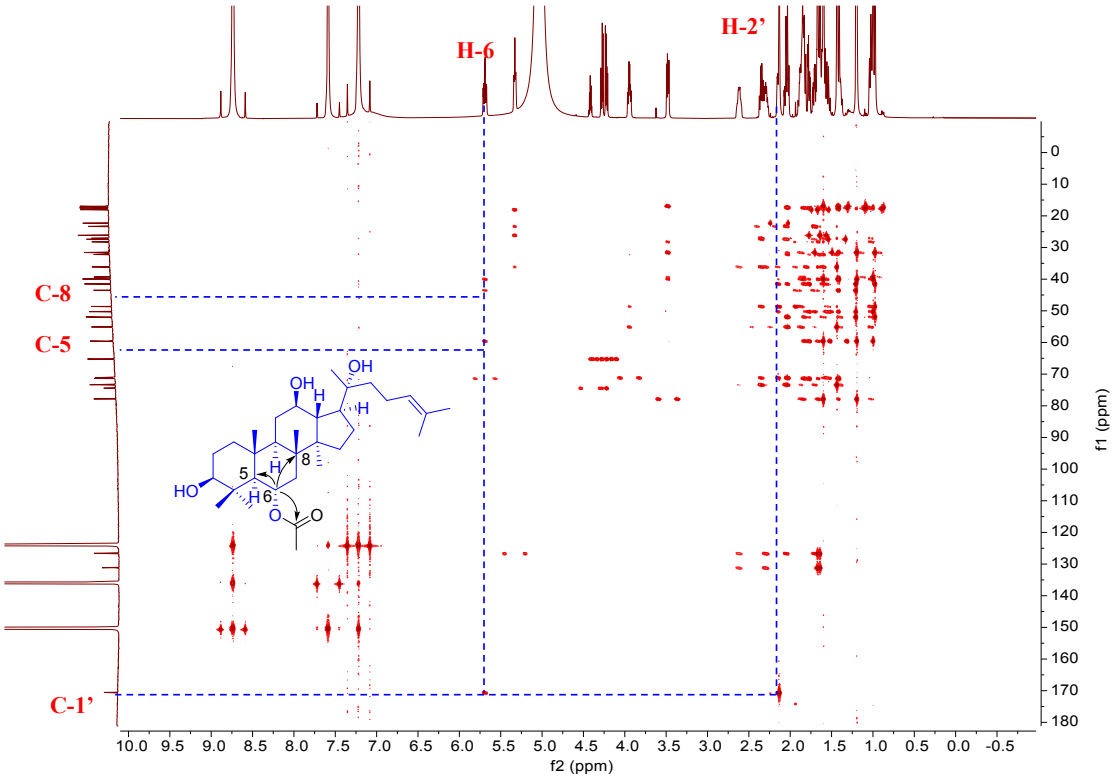

Figure S40 HMBC spectrum of **2a** in pyridine-d_5 (600 MHz).

REFERENCES

(1) Feng L.; Ji S.; Qiao X.; Li Z.; Lin X.; Ye M. *Adv. Synth. Catal.* **2015**, *357*, 1928-1940.

(2) Harley C. B.; Chin A. C.; Akama T.; Ip N. Y.; Wong Y.; Miller-Martini M. U.S. Patent 9248088B2, **2016**.

(3) Zheng S.; Liu D.; Ren W.; Fu J.; Huang L.; Chen S. *EVID-BASED COMPL ALT* **2014**, 843923.

(4) Fu L.; Ye F.; Feng Y.; Yu F.; Wang Q.; Wu Y.; Zhao C.; Sun H.; Huang B.; Niu P.; Song H.; Shi Y.; Li X.; Tan W.; Qi J.; Gao G. F. *Nat. Commun.* **2020**, *11*, 4147.

(5) Sabbatini P.; Filipponi P.; Sardella R.; Natalini B.; Nuti R.; Macchiarulo A.; Pellicciari R.; Gioiello A. *Molecules* **2013**, *18*, 10497-10513.

(6) Wang K.; Zhang X.; Ge Y.; Ju X. *Chemical World* **2007**, *48*, 278-282.

(7) Zhu X.; Tsumagari H.; Honbu T.; Ikeda T.; Ono M.; Nohara T. *Tetrahedron Lett.* **2001**, *42*, 8043-8046.

(8) Bontpart T.; Cheynier V.; Ageorges A.; Terrier N. *New Phytol*. **2015**, *208*, 695-707.

(9) Jones D.T.; Taylor W.R.; Thornton J.M. *Comput Appl Biosci* **1992**, *8*, 275-282.

(10) Kumar S.; Stecher G.; Tamura K *Mol. Biol. Evol.* **2016**, *33*, 1807-1874.